Chapter 8
Modulating Retroreflector-based Free-space Optical (FSO) Communications

Arun K. Majumdar

8.1   Introduction

In this chapter, the niche area of free-space laser communications and data links which use modulating retroreflectors, or retro-modulators, will be discussed. This is a growing area of interest since technology can now support "shutters" that can achieve usable communications rates. Retro-modulators require very little power draw and offer extremely small form factors and mass. The chapter would be structured as follows:

1. Introduction and Background
2. Description of Modulating Retroreflector Free-Space Optical Communications System
3. Modulating Retroreflector Technologies
4. Modulated retroreflector (MRR)-based FSO Communications Systems Performance Analysis
5. Applications

8.2   Introduction and Background

Novel photonics components and devices provide new opportunities for free-space optical (FSO) communications for various applications offering flexibility and mobility. At the same time, there is an increasing demand for high data-transfer rate, light weight, power, and size for communication terminals, establishing multiple communications nodes and mobility. Some of these nodes may be located in remote areas operating in harsh environment without electric power. New sensors capable of generating large amounts of data are needed for fast information transfer. Retrocommunication, i.e., communications with retro-modulation is attractive in these cases where semi-passive optical nodes operating by retro-modulation are more suitable than conventional transceivers implementations. Conventional FSO communications requires each terminal to have a relatively complex point-and-track

system, leading to high cost. While conventional FSO uses similar terminals on both ends of the link, links to MRR are asymmetric links. The MRR makes the bidirectional nature of a typical communication link into a one sided alignment problem. A retroreflective communications system comprises a laser transmitter/ receiver station and a remote retroreflector that can be switched "on" and "off" states. A retro-modulator is potentially less complex and more reliable than a traditional FSO system offering the advantage of significantly reducing the size, power, and weight of hardware required at the remote site for FSO communications while maintaining some of the advantages.

Retrocommunication is based on the principle that an interrogating laser is used to extract information from a remote retroreflector that can be switched "on" and "off" states. The interrogating laser illuminates the remote station where the laser light is modulated and reflected (in the same direction) back to the transmitting unit equipped with an associated detector (receiver) recovering the data signal originated from the remote retro-modulator. Note that one of the terminals can have a relatively complex and expensive laser transmitter and receiver coupled to a point-and-track system. The other terminal can have a retroreflector located behind an optical modulator. The remote terminal can only communicate when it is interrogated by a laser transmitter. The incoming light is first modulated in accordance with the input data stream, and then retroreflected directly back to the remote receiver (located at the interrogating laser site). The modulated reflected light can then be interpreted as a stream of bits recovering the data information. The MRR system can be very compact, light and very cheap as it has no laser and no tracking unit. The concept also opens up the possibility of designing a point-to-multiple-point communications with the local hub comprising the laser interrogator and many distributed MRR modules.

Like the conventional FSO communication system, the FSO communications by MRR also suffer similar optical signal propagation problems due to atmospheric effects in different weather conditions. The clear understanding of atmospheric effects due to absorption, scattering, and turbulence for different geographical locations is necessary in order to deploy these MRR systems for successful FSO communications. Furthermore, it is important to understand the two-way (double-folded) propagation path characteristics for MRR propagation compared to one-way path in conventional communication link. The signal loss, fluctuations or distortion due to the dynamic atmospheric channel will be also dominant factors for MRR FSO communications.

Modulating retroreflective FSO communications has several desirable features which make it an interesting technique for use in many future applications. Some of the advantages are: potential for achieving high-capacity secure communications with low weight (~10–100 g) and small volume, low energy/power consumption (less than 100 mW), a large field-of-view (FOV) resulting in reduced pointing requirements for the interrogating laser transceiver, and no active laser transmitter required by the MRR.

8.3   Description of MRR FSO Communications System

A FSO system using a modulating retroreflector typically consists of a transmitter and receiver (transceiver) and an MRR. The transceiver usually contains a laser source (interrogator), a photodetector, optics, and a module that performs acquisition and tracking (it points the laser towards the MRR unit). The MRR consists of a retroreflector (e.g., a corner cube) and a modulator. Depending on the type of the retro-modulator, the characteristics (such as intensity or polarization) of the reflected beam back to the interrogator is changed when the input voltage applied to the modulator is changed (according to the input data stream). FSO links to MRRs operate differently from conventional point-to-point links, see Fig. 8.1a. Typical point-to-point links use similar terminals on both ends of the link (i.e., a transceiver at both ends) and the communications can be two-way, simultaneously as needed. Links to modulated retroreflectors are asymmetric links which are composed of two different terminals: one end of the link there is the MRR and the opposing terminal is a laser interrogator, see Fig. 8.1b. The interrogator illuminates with a continuous waveform (CW) beam out to retroreflector thus providing the forward link. The purpose of the interrogation beam is thus to supply the necessary optical power for the return signal. The MRR modulates the CW beam with the input data stream, and the beam is retroreflected back in the exact same direction of the interrogator laser. The interrogator receiver then collects the return beam and reconstructs the data stream. This operation of optical retroreflector link is basically in half-duplex (HDX) mode. If bidirectional or full-duplex (FDX) data transfer is desired, a photodetector can be added to the MRR terminal to receive HDX data from the interrogator. For bidirectional data transfer, the MRR modulates the beam with data stream only when the interrogator beam is CW (no data present). Thus both the terminals share interrogator beam as the communication terminal, each as a HDX mode. The FDX operation using MRR (see Fig. 8.1c) will be discussed in details in a later section of this chapter.

8.4   MRR Technologies

In MRR communications various researchers have presented retroreflector designs using either electro-optic phase modulators, acousto-optic modulators, or microelectromechanical modulators (MEMs). The acousto-optic and electro-optic phase modulators are undesirable for FSO communications links due to their sensitivity to atmospheric phase errors. Another type of modulators based on electro absorption in semiconductor multiple quantum well (MQW) structure is also described recently. The MEMs modulators have low reflectivity. The various types of retro-modulation technologies and their basic principles of operation are discussed in this section.

   FSO communications modulators are different from the optical fiber communication modulators. Typical fiber communication modulators are waveguide based
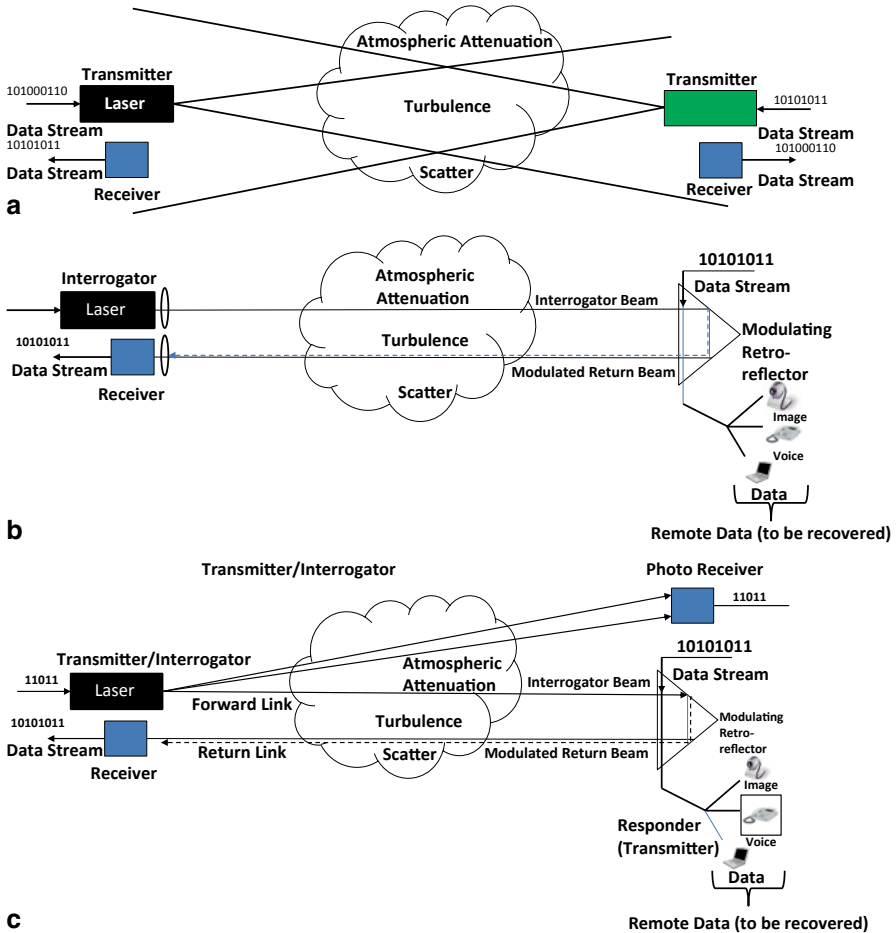
Fig. 8.1 FSO communication system. **a** Conventional FSO communication system. **b** MRR-based FSO communication system (half-duplex, HDX mode). **c** MRR-based FSO communication system concept (full-duplex, FDX mode). *FSO* free-space optical, *MRR* modulated retroreflector

with signals propagating parallel to the modulator surface with physical cross sections are in the order of a few micrometers so that the performance of gigabit speed can be achieved. In an FSO communication modulator, optical signals propagate normal to the modulator surface with cross section in the order of a few milimeter. The modulation speed therefore depends on the fabrication and integration, and is limited by these factors. To achieve multi-gigabit speeds and higher is a challenge for designing a modulator for free space optical communications. Other factors for FSO modulators will include power consumption, size and weight, robustness, and the adaptability with the modulation formats appropriate for communications through dynamic atmosphere. This section will describe below some of the optical

modulator technologies which are applicable to FSO communications. A number of technologies have been proposed, investigated, and developed for the modulation component which include electro-optic modulators (EOMs), acousto-optic modulators (AOMs), and micro-electromechanical modulators system (MEMS).

8.4.1   EOMs

EOM is an optical device in which the optical properties such as power, phase, or polarization of a laser beam change with an electrical signal. Basically the optical properties of the material of the electro-optic devices are altered with an applied voltage in a controlled way. The changes in the optical properties of a material, particularly the permittivity tensor translates into a modification of some parameter of a light wave carrier, for example, phase, amplitude, frequency, polarization, or position, as it propagates through the device. A few materials commonly used for EOM modulators are lithium niobotae (LiNbO$_3$), potassium dihydrogen phosphate (KDP), and gallium arsenide (GaAs).

The operation and application of electro-optic devices rely on the phenomenon of birefringence that is induced by application of voltage to a crystal. In a birefringent crystal an incident light ray will separate into two rays that may travel in different directions depending on its polarization. The material thus has two different indices of refraction, one for each of the two perpendicular components of polarization. Modulator devices for FSO applications can be designed using the following properties of the light wave varied in a controlled way: phase, polarization, amplitude, and frequency, and typically exhibits optimum performance at a single wavelength with some degradation in performance with wideband lasers. For communications purpose, the devices can be used in analog or digital modulation formats and the choice is dictated by the system requirements. Modulation bandwidths extending into the gigahertz range are possible. While analog modulation requires large signal to noise ratio (SNR) limiting its use to narrow-bandwidth, short-distance applications, digital modulation is more applicable to large-bandwidth and longer distance systems.

Basic Principles of Electro-Optics

a.   Pockels and Kerr effects

When an electric field E is applied, the refractive index of an electro-optic medium $n(E)$ is a function of E which can be expanded in a Taylor's series [1] about $E=0$,

$$n(E) = n + a_1 E + \frac{1}{2} a_2 E^2 + \dots, \tag{8.1}$$

where the coefficients of expansion are $n = n(0)$,

$$a_1 = (dn/dE)\big|_{E=0} \text{ and } a_2 = (d^2 n/dE^2)\big|_{E=0}$$

Writing the Eq. (8.1) in terms of electro-optic coefficients $r = -2a_1/n^3$ and $s = -a_2/n^3$

$$n(E) = n - \frac{1}{2} r\, n^3 E - \frac{1}{2} s\, n^3 E^2 + \dots, \qquad (8.2)$$

The second and higher-order terms of the Eq. (8.2) are typically many orders of magnitude smaller than the n. The terms higher than the third can be neglected. The values of r and s depend on the direction of the applied electric field and the polarization of the light.

Pockels Effect In some of the materials when the third term in the Eq. (8.2) is negligible in comparison with the second which varies linearly with E as follows,

$$n(E) \approx n - \frac{1}{2} r\, n^3 E \qquad (8.3)$$

The medium is then known as a Pockels medium and the coefficient r is called the Pockels coefficient. Changes in the refractive index induced by electric fields are very small. Some of the common crystals used as Pockels cell include $NH_4H_2PO_4$ (ADP), KH_2PO_4 (KDP), and $LiNbO_3$ [1].

Kerr Effect In some materials which are centrosymmetric, *n(E)* is an even symmetric function (invariant to the reversal of *E,* and the coefficient *r* in Eq. (8.2) is zero), so that the Eq. (8.2) can be written as

$$n(E) = n - \frac{1}{2} s\, n^3 E^2 \qquad (8.4)$$

If the material shows this property, it is then called a Kerrr medium.

Phase Modulation

The principle behind the phase modulation is to use a crystal, such as Lithium niobate, whose refractive index is a function of the strength of the local electric field and therefore the light will travel more slowly through the crystal when exposed to an electric field. By changing the electric field in the crystal, the phase of the laser light exiting the EOM can therefore be controlled by changing the electric field in the crystal. A light wave can be phase modulated using an electro-optic crystal and an input polarizer in the proper configuration. The phase of the light leaving the crystal is directly proportional to the length of time for the light to pass through it. Figure 8.2 describes the concept of Phase Modulation process. An applied voltage *V* will rotate the principal axes in the crystal cross section with the light polarized along the new axis x′ principal axis when the modulation voltage *V* is applied. The input polarizer is aligned parallel to one of the principal axes when the voltage is on or off.
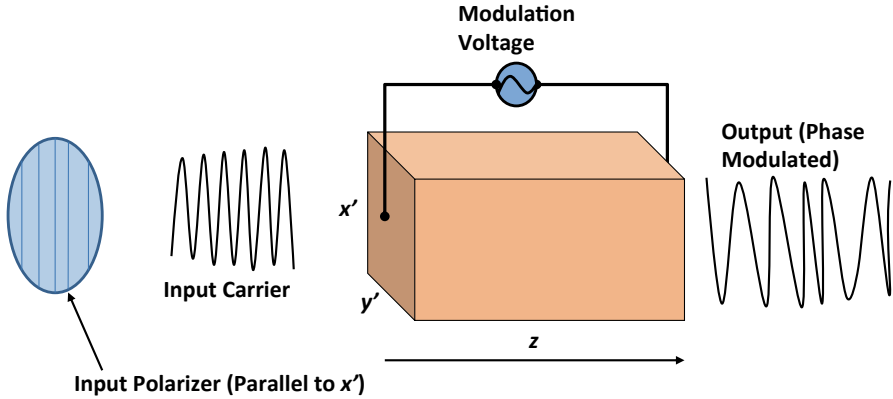
Fig. 8.2 A phase modulator (longitudinal): the light polarized along the new x′ principal axis, V is the modulation voltage applied, output light is phase modulated

Figure 8.2 indicates a polarizer along x′ axes with an input optical electric field $E_{ix'}(t) = E_i \cos \omega t$. The output electric field at the output of the crystal at $z = L$ is then [2]

$$E_o(t) = E_i \cos(\omega t - \varphi) \tag{8.5}$$

where the total phase shift,

$$\varphi = \frac{2\pi}{\lambda}(n_{x'} + \Delta n_{x'})L = \varphi_0 + \Delta\varphi_{x'} \tag{8.6}$$

In the above equation, the natural phase term $\varphi_0 = \frac{2\pi}{\lambda}Ln_{x'}$ ($n_{x'}$ is the unperturbed index in the x' direction), and the electrically induced phase term, $\Delta\varphi_{x'} = \frac{2\pi}{\lambda}L\Delta n_{x'}$ for a polarization in the x' direction. $\Delta n_{x'}$ is the change in the index is $\Delta n_{x'} \approx \frac{1}{2}n_{x'}^3 \cdot rE$ (r is the electro-optic coefficient of the EOM). Substituting the value of the change in index, the induced phase shift can be written as $\Delta\varphi_{x'} = \frac{\pi}{\lambda}n_{x'}^3 r\ V$, where the modulation voltage V is related to the applied electric field E by $E = V/L$. Note that $\Delta\varphi_{x'}$ is independent of L and is linearly dependent on L. For a transverse modulator (where the voltage is applied in a direction perpendicular to the direction of light propagation) $E = V/d$ (d is the transverse dimension), and the induced phase shift is then given by $\Delta\varphi_{x'} = \frac{\pi}{\lambda}n_{x'}^3 r\ V\left(\frac{L}{d}\right)$ (a function of the aspect ratio $\frac{L}{d}$ and the voltage V).

The applied voltage at which the induced phase shift changes by π is known as the *half-wave voltage*. This is obtained when $\Delta\varphi_{x'} = \pi$ which for longitudinal modulator is $V_\pi = \lambda/n_{x'}^3 \cdot r$ and for a transverse modulator is $V_\pi = (\lambda/n_{x'}^3 r)\,(d/L)$.

If a direct current (DC) voltage is used, a crystal and the orientation can have two possibilities: (i) the crystal having principal axes which will not rotate with applied voltage V, and (ii) the crystal having a characteristic plane perpendicular to the direction of propagation. If a field is applied such that the axes rotate in this plane, the input wave must be polarized along one of the new principal axes. In that case, it will always be polarized along a principal axes, whether the voltage is on or off. By turning the voltage on or off, phase modulation can be achieved.

When a sinusoidal modulation voltage is applied ($V = V_m \sin \omega_m t$), the corresponding electric field is ($E = E_m \sin \omega_m t$). The total phase shift in this case is

$$\varphi = \frac{2\pi}{\lambda}\left(n_{x'} - \frac{1}{2} n_{x'}^3 \cdot rE_m \sin \omega_m t \right) L = \frac{2\pi}{\lambda} n_{x'} L - \delta \sin \omega_m t \qquad (8.7)$$

The parameter δ is known as the phase modulation index or depth-of-phase modulation, and is given by $\delta = \left(\dfrac{\pi}{\lambda} \right) n_{x'}^3 \cdot rE_m L = \pi V_m / V_\pi$. If we neglect the constant phase

term, φ_0 and using the Bessel function identity

$$\cos(\delta \sin \omega_m t) + j \sin(\delta \sin \omega_m t) = \exp[j\delta \sin \omega_m t] = \sum_{l=-\infty}^{\infty} J_l(\delta) \exp[jl\omega t], \qquad (8.8)$$

the output light wave is then given by [2]

$$\begin{aligned} E_0(t) = E_i[& J_0(\delta) \cos \omega t + J_1(\delta) \cos(\omega + \omega_m)t - J_1(\delta) \cos(\omega - \omega_m)t \\ & + J_2(\delta) \cos(\omega + 2\omega_m)t + J_2(\delta) \cos(\omega - 2\omega_m)t + \dots] \end{aligned} \qquad (8.9)$$

The output therefore consists of components at frequencies ω and $(\omega + n\omega_m)$, $n = \pm 1$, $\pm 2, \dots$.

If there is no modulation, $\delta = 0$ and $J_0(0) = 1$, $J_n(0) = 0$ for $n \neq 0$, and $E_0(t) = E_i \cos \omega t = E_{i_{x'}(t)}$. For $\delta = 2.4048$, $J_0(\delta) = 0$ which means all the power is transferred to harmonic frequencies.

Polarization Modulation

The type and orientation of the nonlinear crystal, and the direction of the applied electric field can determine the phase delay which depends on polarization direction. A Pockels cell can be used for modulating the polarization state. For a linear input polarization (often oriented at 45° to the crystal axes), the output polarization will in general be elliptical, rather than simply a linear polarization state with a rotated direction. Change of the input polarization state at the output occurs by coherent addition of two orthogonal waves which can be termed as polarization modulation. For example, for a longitudinal polarization modulator, the input polarizer can be oriented along the x′ principal axis at 45° with respect to the perturbed x′ and y′ axes. The input light wave is decomposed equally into the two orthogonal linear

eigen polarizations along these axes. If the light is polarized along the x axis and propagates along the z principal axis (representing the fast and slow axes x' and y'), the propagating fields can be written as

$$E_{x'} = E_0 \cos\left[\omega t - \left(\frac{2\pi}{\lambda}\right)n_{x'}z\right]$$

$$E_{y'} = E_0 \cos\left[\omega t - \left(\frac{2\pi}{\lambda}\right)n_{y'}z\right]$$

(8.10)

The refractive indices along these two fast and slow axes are

$$n_{x'} \approx n_x - \frac{1}{2}r_x n_x^3 E = n_x - \Delta n_x$$

(8.11)

$$n_{y'} \approx n_y - \frac{1}{2}r_y n_y^3 E = n_y - \Delta n_y$$

In the above equation, n_x, n_y are the indices in absence of an applied field, and r_x, r_y are the electro-optic coefficient for the EOM with the orientation of the applied voltage. A phase difference or retardation Γ results between the two polarizations propagating at different speeds through the crystal which is given by [2]

$$\Gamma = \frac{2\pi}{\lambda}\left(n_{x'} - n_{y'}\right)L = \frac{2\pi}{\lambda}\left(n_x - n_y\right)L - \frac{\pi}{\lambda}\left(r_x n_x^3 - r_y n_y^3\right)EL = \Gamma_0 + \Gamma_i$$

(8.12)

where Γ_0 is the natural phase retardation in the absence of an applied voltage, and Γ_i is the induced retardation due to the applied voltage V. The optical fields at the output can be expressed in terms of retardation Γ is

$$E_{x'} = \cos \omega t$$
$$E_{y'} = \cos(\omega t - \Gamma)$$

By applying the appropriate voltage magnitude, the output polarization can thus be controlled. In the absence of natural birefringence, $n_x - n_y = 0$, the half-wave voltage V_π is defined as the voltage that would produce a retardation of $\Gamma = \Gamma_i = \pi$. In this case, a vertical polarization input becomes a horizontal polarization output. The total retardation in terms of V_π (calculated assuming no birefringence) is

$$\Gamma = \Gamma_0 + \pi\left(\frac{V}{V_\pi}\right)$$

(8.13)

In order to achieve polarization modulation, a birefringence must exist in the crystal cross section. For a characteristic plane cross section, the input polarization propagates through the crystal unchanged with no applied voltage ($V=0$). With the applied voltage causes the axes to rotate 45° in the cross section with respect to the input polarization, and the input will decompose into two equal components and

finally change polarization state at the output. For the cross section with natural birefringence, the input polarization state will change with $V=0$ as well as with an applied voltage.

Amplitude Modulation

Combined with other optical elements, in particular with polarizers, Pockels cells can also be used for other kinds of modulation such as amplitude modulation. An amplitude modulator is based on a Pockels cell for modifying the polarization state and a polarizer for subsequently converting this into a change in transmitted optical amplitude and power. A quarter ($\lambda/4$) wave plate introduces a bias to produce linear modulation. The ratio of output to input intensity, i.e., the transmission $T=I_0/I_i$ is the relevant parameter for intensity modulator parameter. The transmission for this modulator is given by

$$T(V) = sin^2(\Gamma/2) = sin^2\left(\frac{\Gamma_0}{2} + \frac{\pi V}{2V_\pi}\right) \tag{8.14}$$

To accomplish linear modulation, a fixed bias of $\Gamma_0 = \dfrac{\pi}{2}$ must be introduced by placing an additional phase retarder, e.g., a quarter ($\lambda/4$) wave plate at the output of the electro-optic crystal. For a sinusoidal modulation voltage $V = V_m \sin\omega_m t$, the retardation at the output of the crystal is

$$\Gamma = \Gamma_0 + \Gamma_i = \frac{\pi}{2} + \Gamma_m \sin\omega_m t \tag{8.15}$$

where $\Gamma_m = \dfrac{\pi V_m}{V_\pi}$ is the amplitude modulation index or depth-of-amplitude modulation. The transmission in this case can be written as [2]

$$T(V) = sin^2\left(\frac{\pi}{4} + \frac{1}{2}\Gamma_m \sin\omega_m t\right) = \frac{1}{2}\left[1 - \cos\left(\frac{\pi}{2} + \Gamma_m \sin\omega_m t\right)\right] \tag{8.16}$$

$\approx \dfrac{1}{2}\left[1 + \Gamma_m \sin\omega_m t\right]$ when $V_m \ll 1$, and $\Gamma_m \ll 1$ (i.e., small modulation voltage and modulation depth): the transmission or output intensity is linearly related to the modulating voltage.

8.4.2   AOModulation

In this case, a light field is modulated by an acoustic signal. The modulator is an acousto-optic crystal, which means that the refractive index depends on the pressure. Sound waves are simply the variation of pressure resulting in a variation of refractive index. As the sound wave travels through the crystal, there are regions

of high and of low refractive indexes due to the difference of pressure, depending on the sound. The acoustic wave creates a diffraction grating and we have a spacing created in the material. AOM introduce a periodic modulation of the refractive index in a transparent medium, of which light is scattered similar to the Bragg diffraction.

The periodic index modulation is generated by sound waves which form a periodic density grating when propagating through the medium. The sound waves are created by a Piezo electric transducer driven by a radio frequency (RF) signal. An acoustic absorber on the other end of the crystal prevents the acoustic wave from travelling back to the transducer. The laser beam changes its direction slightly due to Bragg diffraction. One has to distinguish between the "transmission" in the original beam direction and the "efficiency" which gives the fraction of the original beam diffracted into the first order beam. The intensity of the sound wave determines the efficiency of the AOM and is therefore used to modulate the light intensity. The switching speed of an AOM is limited by the time the sound wave needs to cross the beam diameter. In order to achieve high-speed modulation, the beam diameter has to be small. The light intensity and the laser induced damage threshold of the modulator will therefore have to be optimized. The light is scattered from a moving refractive index grating, which generates a slight frequency shift of the diffracted light, equal to the frequency of the sound wave. The movement of the acoustic wave is like a moving diffraction grating and the frequency of the diffracted beam is Doppler shifted by $\pm f_m$, a frequency modulation of light.

An AOM operating in the Bragg regime can be used in actual pass configuration to achieve a high-speed frequency MRR. The Bragg diffraction condition is given by

$$2\lambda_S sin\theta_B = \lambda_L \tag{8.17}$$

where λ_S is the acoustic wavelength in the AOM crystal, θ_B is the Bragg angle, and λ_L is the wavelength of the laser. The incident beam undergoes mirror-like reflection from the acoustic wave front where the diffracted beam and the incident beam are in phase over the entire acoustic wave front. Figure 8.3 illustrates the basic concept of the AOM-based retroreflector.

The interrogating laser beam is diffracted by the AOM device when a sequence of RF pulses (representing the data stream) is applied to the AOM. The diffracted beam is retroreflected through the AOM towards the laser interrogator, and the return signal can be detected by the presence or absence of frequency modulation [3]. The data transmission rate is determined by the spacing between pulses which requires that the rise time of the diffracted optical pulses from the AOM and the RF pulse width should be comparable or smaller than the spacing between pulses. A 1 MHz data transmission rate in Bragg regime was demonstrated [3] which requires an RF power of ~2 W, and the weight and volume of the modulator package are ~1 kg and ~3,000 cm^3, respectively. The researchers suggested potential rate to be ~1 GHz in the Raman-Nath regime and can be suitable for free space laser communications.
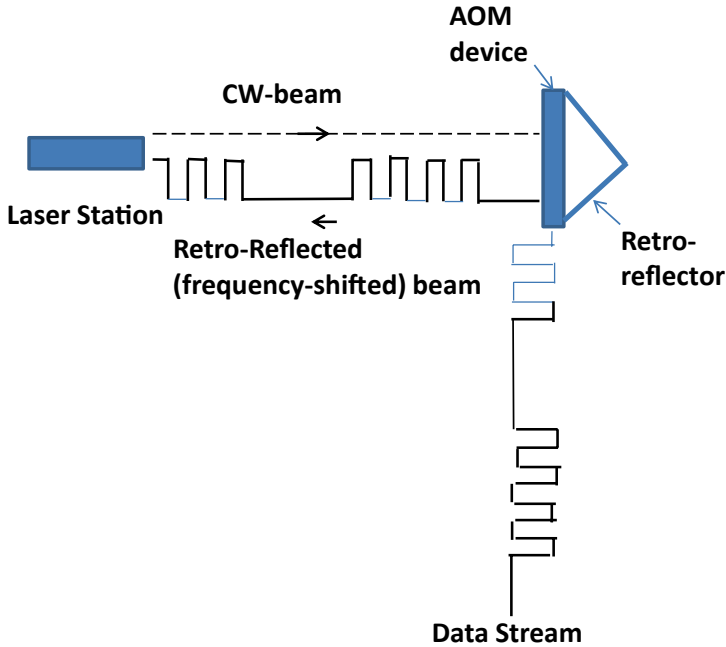
Fig. 8.3 Concept of AOM-based modulating retroreflector for FSO communication: CW-laser beam from the interrogator is incident on the AOM device and frequency-shifted beam is retroreflected towards the interrogator (*Reprinted with permission from NRC Research Press © 2003, Fig. 1, p. 627* [3]). *AOM* acousto-optic modulator, *FSO* free-space optical, *CW* continuous waveform

The AOM-based device may be suitable for certain forms of high-speed FSO communications because of its simplicity of the optical setup to establish an FSO communication link with a remote link. Devices based on electro-optic phase modulation can be used for applications involving high-speed (GHz) FSO communications where the MRR can be mounted on a moving platform such as a satellite or an unmanned aerial vehicle (UAV). The retroreflected signal can be detected with an adequate signal-to-noise-ratio using heterodyne detection technique.

8.4.3   Liquid Crystal (LC)/Ferroelectric Liquid Crystal (FLC)-based Modulators FLC Modulators

Liquid crystal (LC) materials are in a state in-between solid and liquid which under some conditions have an anisotropic order but still maintain an ability to flow. There are three phases of the LC: smectic, nematic and cholesteric. The smectic phase structure is closet to the solid state with translational and orientation order, the nematic LCs only have directional order and no long-range spatial structure, and the cholesteric comes from a nematic LC with chiral molecules (different from its

mirror image) acquiring a helical distortion. For electro-optic applications LCs with nematic phase are widely used. The nematic crystal has a useful property that the dielectric anisotropy, $\Delta\varepsilon = \varepsilon' - \varepsilon''$ (where ε' and ε'' are the two different dielectric constants for the dielectric tensor ε) causes the LC to interact with an external applied electric field. With positive dielectric anisotropy the average direction of the material will orient as to align with the electric field, whereas when the electric field is removed the elasticity causes the material to relax back to its initial equilibrium state. Modulation modes of nematic LCs can be described in the following way. Different modulation modes for the LC device can be realized and will depend on the alignment layers, the direction of the external electric field and the polarization of the incoming light. For the directors parallel to the alignment layers and without any twist, pure phase and combinations of phase and amplitude modulation can be achieved [4]. The complex modulation for different angles of the polarizer, α, and various delays can be calculated. Pure phase modulation can be achieved when the polarization of the incoming light is aligned with the optical axis of the LC, i.e., $\alpha=0$, whereas for light polarized perpendicular to the optical axis, i.e., $\alpha=90°$, the LC will not alter the polarization or the phase of the light. For all other angle, i.e., $0°<\alpha<90°$, the polarization state will be changed resulting in an amplitude loss at the second passage of the polarizer. When the polarizer is set to $\alpha=45°$, optimal intensity modulation can be achieved but not with totally pure amplitude modulation.

Electro-Optical Properties of FLCs   Unlike nematic types FLCs exhibit a net dipole over the bulk of the material and because of their electrical polarization properties may switch very quickly under a DC field. Ferroelectrics are chiral smectic C devices, i.e., they have a layered structure with the molecules at some angle (the "cone angle") away from the layer normal. Also there is some inherent twist in the structure. The Surface Stabilized Ferroelectric Liquid Crystal (SSFLC) configuration is the most common configuration for FLC device. In this case the natural twist of the material is suppressed by the surface conditions. When a DC voltage is applied across the display substrates the molecules rotate around the cone so that in the center region the direction the molecules are pointing changes in the plane of the cell by about 45°. Thus the direction of the ferroelectric can be switched very quickly from being along the polarization direction of incident light to being 45° from the polarization direction of the light. Using a ferroelectric material retarding the light by a half wave, the state of the light on reaching the exit polarizer may be changed from 0° to 90° achieving a black and white operation.

LC operating as an Optical Shutter   For MRR-based FSO communications applications, normally a laser interrogator sends the light beam towards the MRR which has LC modulator in front of a retroreflector. The MRR sends back the incoming signal towards the interrogator with the modulated information. Shutters using FLC technology offer the speed of the electronic shutters (<100 μs) on large diameters with added advantage of having the vibration free LC shutters. Figure 8.4 illustrates the FLC-based optical switch: voltage between the electrodes switches the orientation of the FLC molecules optic axis in one of the two states, and thus the polarization of the outgoing light is changed.
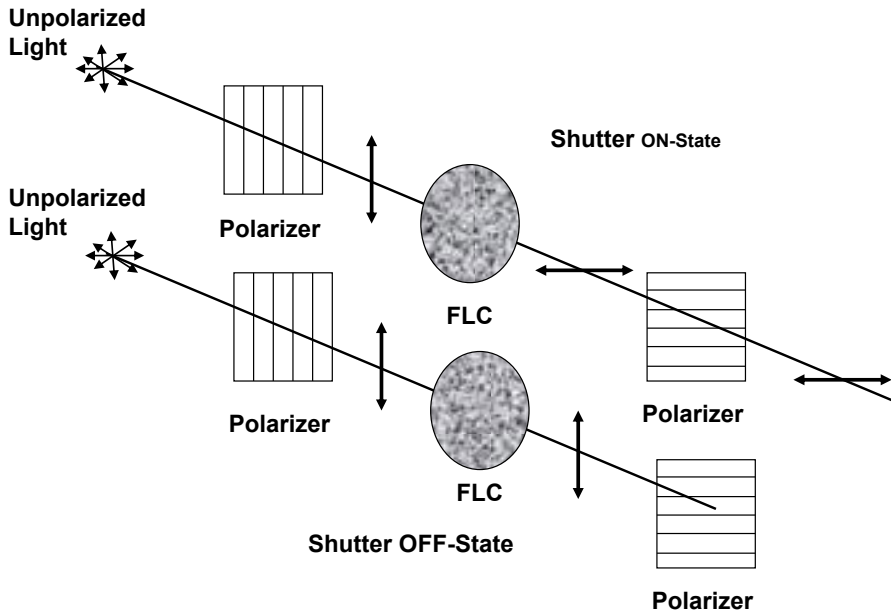
Fig. 8.4 Concept of FLC-based optical switch: voltage applied between the electrodes switches the orientation of the FLC molecules optic axis in one of the two states, changing the polarization of the outgoing light. *FLC* ferroelectric liquid crystal

FLC cells act as optical shutters when placed between linear cross polarizers or alternatively by using a polarized light source and one linear polarizer. Figure 8.5 shows how the molecular orientation is tilted by an angle θ with respect to the normal to the layers (the x-axis) exhibiting the ferroelectric properties. When placed between two closed glass plates the surface interactions permit only two stable states of molecular orientation at the angles ±θ. Applying either a +E or −E electric field in the z-direction, the molecular orientation can be switched into the stable state of either +θ or −θ and therefore the optic axis may thus be switched between two orientations. If the incident light is linearly polarized at an angle θ with the x-axis, the polarization is parallel to the optic axis for +θ state. The wave travels in this case with the extraordinary refractive index n_e without retardation. In the −θ state, the plane makes an angle 2θ with the optic axis. For 2θ=45°, the retardation is given by [1]

$$\Gamma = 2\pi(n_e - n_0)d/\lambda_0 \tag{8.18}$$

where d=the thickness of the FLC cell, and n_0 is the ordinary refractive index. When $\Gamma = \pi$, the plane of polarization rotates 90° which means that by reversing the applied electric field, the plane of polarization can be rotated by 90°. When the FLC cell is placed between two crossed polarizers, an intensity modulator can be designed. The response time of FLC switches is typically <20 μs at room tem-
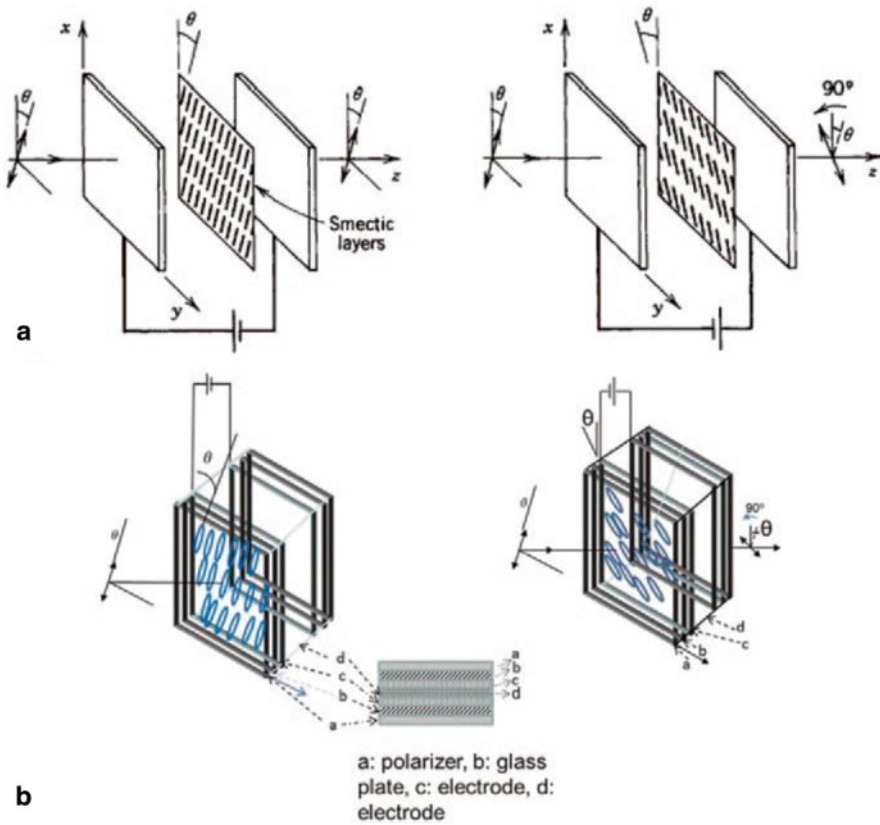
Fig. 8.5 a FLC molecular orientation at the angles $+\theta$ or $-\theta$ by applying electric fields $+E$ or $-E$, thus showing the switching capability between two orientations (*Reprinted with permission from John Wiley & Sons, Inc. 1991* [1]. **b** The schematic of FLC when placed between two closed glass plates. *FLC* ferroelectric liquid crystal

perature which is much faster than that of nematic LCs. The switching voltage is typically ± 10 V.

8.4.4   MQW Technology for Modulation MQW Modulators

Concepts and basic principles of operating MRR devices using MQW technology offers a number of advantages compared to other types of MRR technology. Some of the advantages are: low power consumption (milliwatts, less than 1 W), low mass, compact and capable of high switching speeds (e.g., ≈ 45 Mbps in FSO communications). The working principle of MQW is based on electro absorption in semiconductor MQW and uses the stark effect to vary the absorption of a trans-
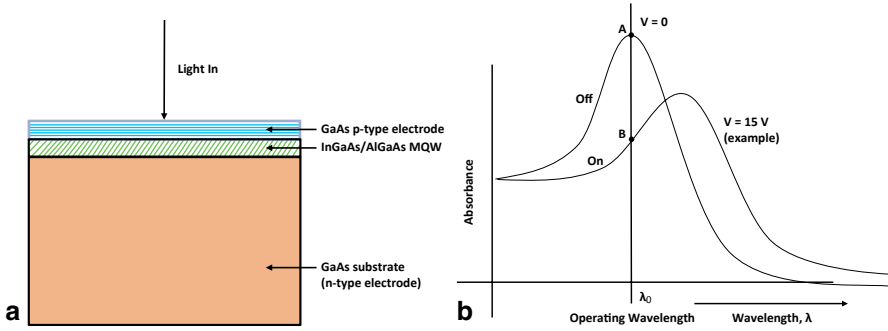
Fig. 8.6 a MQW schematic: GaAs material grown in alternating layers with active regions about one micron thick. **b** Typical characteristics: contrast ratio changes from no-voltage ($V=0$) to a moderate voltage (~ 15 V) at an operating wavelength λ_0 (interrogator laser wavelength). *MQW* multiple quantum well

missive crystal window where absorption of materials changes in response to an electric field, absorption peak remains resolved, and very fast optical modulation in semiconductors (≈ 40 GHz). The devices are basically p-i-n devices mode from In GaAs/AlGaAs using molecular beam epitaxial (MBE) technique [5, 6].

Figure 8.6a shows a schematic of MQW structure. When a moderate voltage ($\approx 2-20$ V) is applied across the device in reverse bias, the absorption characteristics changes causing a shift in wavelength and in magnitude. The transmission of the device near this absorption changes appreciably which then can act as a high speed on-off shutter. The modulators consist of about one hundred very thin (~ 10 nm) layers of several semiconductor materials, such as GaAs, AlGaAs, and In GaAs, epitaxially deposited on large (~ 3-in. diameter) semiconductor wafer [5]. The structure designed this way behaves like a *p-i-n* diode where the thin layers induce a sharp absorption feature at a specific wavelength. Figure 8.6b illustrates how the application of a moderate voltage shifts the transmittance at a given operating wavelength. A signal can be encoded in an On-Off-Keying (OOK) format onto the carrier interrogation beam. The contrast ratio for a MQW modulator can be defined as Imax/Imin (where Imax and Imin are the light intensities at two switching positions for two voltages, i.e., with no-voltage and for some applied voltage). The switching speed depends on the material characteristics and the area of the aperture of the device, and therefore data rates are limited by RC (Resistor Capacitor), time constant (R=sheet resistance $\approx 5-10$ Ω, C≈ 5nF/cm^2). The power consumption is $CV^2 f$ where f is the drive frequency. The device is a trans-missive modulator. The contrast ratio is a function of the drive voltage applied to the device, and increases with the voltage until saturated. Reference [5] describes the modulators to have contrast ratio between 1.7:1 to 4:1 for applied voltage between 15 and 25 V. For FSO communications over 1 km or higher, a large aperture size is needed for accomplishing a reasonable SNR of the received optical power. Also the speed of the MQW shutter depends inversely on the area of the modulator area. Therefore MQW modulator requires proper design for long range, high data rate FSO communications applications. However, a large power penalty may be incurred for large
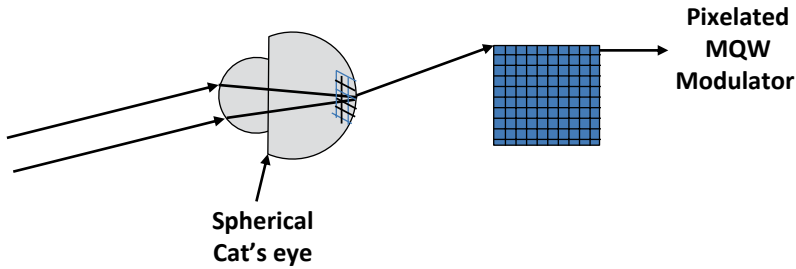
Pixelated MQW Modulator

Spherical Cat's eye

Fig. 8.7 Concept of a "Cat's eye" retro-modulator with pixelated MQW (at focal plane) (*Reprinted with permission from SPIE, 2002,* [10]). *MQW* multiple quantum well

aperture MQW shutter, since electrical power consumption scales as [5]: $D^4_{mod} \cdot V^2 B^2 R_s$, where D_{mod} is the diameter of the modulator, V is the applied voltage, B is the maximum data rate of the device, and R_s is the sheet resistance of the device. Naval Research Laboratory (NRL) has also considered "pixelated" MQW modulator to address these problems. A trans-missive device with nine "pixels" with an overall diameter of 5 mm was achieved to support over 10 Mbps.

The two types of retro reflectors have been considered by NRL for reflecting the incoming light back to the interrogator location: (i) corner cube optical retroreflector, attached at the back of the MQW modulator, and (ii) Cat's eye retro-modulator, where an array of small shutters are placed in the focal plane of optics designed to perform as a retroreflector. In this way a small spot size (mm) allows fast data rates, and the array combined with optics effectively makes the aperture large [7]. The concept of a focal plane "Cat's eye" retro-modulator is illustrated in Fig. 8.7.

MQW-based MRR development, advances, and recent applications State of the art technology based on MQW technology for FSO communications is capable of transmitting data at tens of Mbits/s. NRL has been the pioneer in developing MQW modulators for use in MRR-based FSO communication. NRL demonstrated this technology for various space [8], airborne, and ground applications [9, 10], using 850 nm, 980 nm, and 1.55 μm infrared (IR) wavelengths. Some of the MRR using Cat's eye concept of retroreflector is also discussed here. Results for data-in-flight on a small, UAV at up to 5 Mbps was reported [9]. The device was a corner cube modulator using a 980-nm shutter, with a contrast ratio of 2:1 when driven at 12 V. MQW-MRR using a Cat's eye retroreflector with MQW in the focal plane of the Cat's eye is described [11]. A 10 Mbps free-space link over a range 1 km was demonstrated. Cat's eye MQW MRR have the potential to increase the maximum data rate of the system by more than an order of magnitude over conventional corner cube retro-modulator system. Figure 8.7 illustrates the basic concept of a focal plane "Cat's eye" retro-modulator. By using large number of pixels in the focal plane, increased data rate without decreasing optical aperture or greatly increasing power can be achieved. System field of view and speed can be traded without using a large number of pixels. Cat's eye retroreflectors are best for FSO communications

links requiring high data rates at long range, but with less restriction on space, weight and power. NRL described a Cat's eye-based MRR weighing 410 g (including electronics) for communicating at 10 Mbps in a 4 km link [12] and a new modulator for a laboratory demonstration of a 70 Mbps [11]. The performance of a 1.6 cm flat-focal-plane Cat's eye MRR for a FSO link above the Chesapeake Bay was described using a 5-W laser interrogator to achieve a 45-Mbps data rate over a range of 7 km [13]. An optical modulating retroreflector link to a small robot using an array of 6 MRRs and photodetectors with a FOV of 180 (azimuth)·30° (elevation) was demonstrated [14] out to ranges of 1 km at 1.5 Mbps data rate. NRL also demonstrated MRR laser-com terminal for applications to small UAVs for a maximum range of 2.5 km and the data rate of 2 Mbps [15]. Live video transmission to the ground was achieved. The use of MRRs for high data-rate communication downlinks from small satellites was recently investigated [16]. In this case, a laser ground station would illuminate a retroreflector on-board the satellite while the MRR modulates the reflected signal, there by encoding a data stream on the returning beam which is received by a detector on the ground. Future possibility of using constellations of nano-satellites for a variety of missions is also pointed out.

8.4.5   MEMS Deformable Mirror Retroreflector Modulators

MEMS MRR Concepts This is a class of MRR where a modulating corner-cube retroreflector has one MEMS mirror that is based on deformable mirrors switching from flat reflecting surfaces (no voltage) to diffractive surfaces (with applied voltage) made of deformed mirror. FSO communications system performance has direct impact by the retro-modulator characteristics as follows: wave front aberration and effective optical aperture affect maximum operational range; data bandwidth is determined by modulation response time and contrast ratio; overall system utility; and robustness are determined by operational tolerances including modulator acceptance angle, wavelength range, and ability to withstand physical and thermal shock. In some practical applications, where MRR can be used for remotely data transfer, the communication range is from 0.1 to 10 km but must operate under different atmospheric turbulence conditions. The effective optical aperture must be 1 cm or larger, and the wave front distortion should be below $\lambda/10$. The system should be able to operate over a wide range of incident angles, up to about $\pm 30°$. The wavelength range for operating the communication system is also another important consideration (i.e., the MRR device also has to accommodate the interrogator (transmitting) laser wavelength ranges). The final consideration for designing MRR-based FSO communication system is the data-modulation contrast of 10:1 (desirable; 2:1 required) for an appropriate SNR and the data-modulation rate of at least 100 kHz (data rates as high as 10 s and 100 s of gigahertz will be eventually needed).

MEMS-based retro-modulators have been recently demonstrated which are suitable for low-cost, low-power compact communication over hundreds of meters to
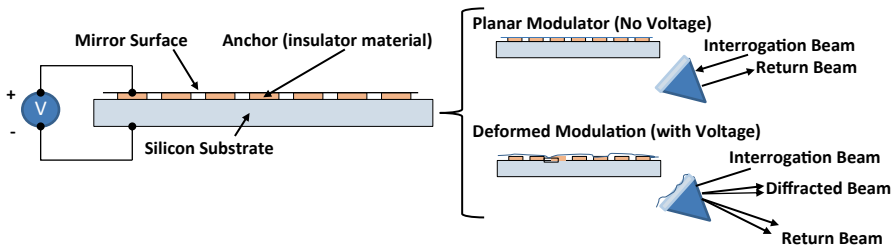
Fig. 8.8 MEMS-based modulating retroreflector (*Reprinted with permission, SPIE, 2009* [17]). *MEMS* micro-electromechanical-system

detect and modulate an incoming (interrogating) laser beam, and then to return the modulated signal to the location of the sender (i.e., towards the interrogator). This type of MRR consists of a MEMS-based electromechanical modulator combined with a passive retroreflector (e.g., a hollow retroreflector where the MEMS modulator serves as one (or more) of the three reflective facets of the retroreflector. The modulator with the MEMS technology can act as a plane mirror (with no applied voltage) maximizing the retroreflected light, or it can be made to act as a non-plane (corrugated or deformed) mirror (with applied voltage), reducing the amount of light that is retroreflected back to the sender. Modulation can be achieved by switching between these two voltages.

Modulation concept for MEMS-based Retroreflector A number of researchers have designed and developed MEMS-based MRR in recent years. For FSO communications applications, some of the concepts and basic working principles of some of these modulators are described in this section. The discussion below considers generally two types of MEMS-based MRR: (i) The first kind MEMS device [17] is based on alternating between a flat state returning most of the incident laser light to the source, and a corrugated (deformed) state acting as a diffraction grating, diverting a significant amount to higher orders (so that the most of the outgoing light does not reach the source), thus depleting the zero order return; (ii) The other kind [18] uses an MEMS deformable micromirror array switching from flat reflective surfaces (no voltage) to diffractive surfaces (with applied voltage) made of hexagonal concave mirror-lenses arrays.

The basic concept of the MEMS-based MRR is shown in Fig. 8.8. The MEMS modulator is a reflective diffraction grating with controllable groove depth. It acts as one of the three mirrors that makes up the corner-cube retroreflector and is capable of modulating a continuous laser beam by switching between an unpowered (no voltage) flat-mirror state to an energized-diffraction state (with input voltage). An electrically modulated deformable MEMS mirror is embedded in a hollow retroreflector [17] which is interrogated by a compact laser transceiver system which operates at a wavelength of 1.55 μm. The MEMS mirror modulates the interrogating laser beam and returns the modulated signal to the interrogating source, where it is decoded. The MEMS modulator uses electrostatic actuation to deform rows of edge-supported narrow plates to form a diffraction grating. The reflective gold

mirror surface supported by a tensile silicon nitride layer is maintained at a ground potential and a voltage is applied to the conductive substrate so that an electrostatic force is generated between those two surfaces resulting in deflection of the flexible mirror surface. This type of actuator can be modeled as a pair of planar electrodes of overlapping effective area *A,* with a spacing *g* (closely-spaced). A voltage *V* is applied between the electrodes which creates an electrostatic attractive force F_e given by [17]:

$$F_e = \frac{\varepsilon_0 A V^2}{2g^2}$$ (8.19)

where ε_0 is the permittivity of air (8.8×10^{-12} F/m). The above equation is modified when the electrodes deflect towards one another by an amount *z*:

$$F_e = \frac{\varepsilon_0 A V^2}{2(g-z)^2}$$ (8.20)

When one actuator electrode is kept fixed but the other movable electrode supported by a mechanically compliant spring having stiffness factor *k,* the mechanical restoring force F_m opposing electrode motion can be expressed by

$$F_m = -kz$$ (8.21)

Equating the electrical and mechanical forces at equilibrium state ($F_e = -F_m$) the applied voltage and the equilibrium deflection *z* are related by [17]

$$V = \sqrt{\frac{2kz(g-z)^2}{\varepsilon_0 A}}$$ (8.22)

The above equation shows the relationship between *g, z,* and *V.* The advantages of using electrostatic actuation to modulate the interrogating laser beam are: the actuators consume practically no power, exhibit no hysteresis, and the MEMS deformable mirrors are easy to fabricate. With no voltage applied to the MEMS modulator, the 0th order intensity of the far-field diffraction pattern contains the return beam of the interrogating illumination system which would have been received from the modulator in the field if it were mounted in a retroreflector assembly. With applied voltage, the modulator deflects and the intensity of the 0th diffraction order decreases while off-axis higher-order diffraction orders increase in intensity. The MEMS mirror can be incorporated as a facet in a hollow retroreflector to return the modulated beam to the interrogator [17].

   The MEMS modulators can have various architectures. One method simply employs phase modulation by moving the retroreflector along the beam direction with MEMS actuators as described in [19]. A spherical Cat's eye retroreflector is used where the mass of the retroreflector is inversely proportional to the resonant frequency at which it can be moved (i.e., limiting the speed of modulation). One of the mirrors in a corner-cube retroreflector replacing with an MEMS actuated grat-
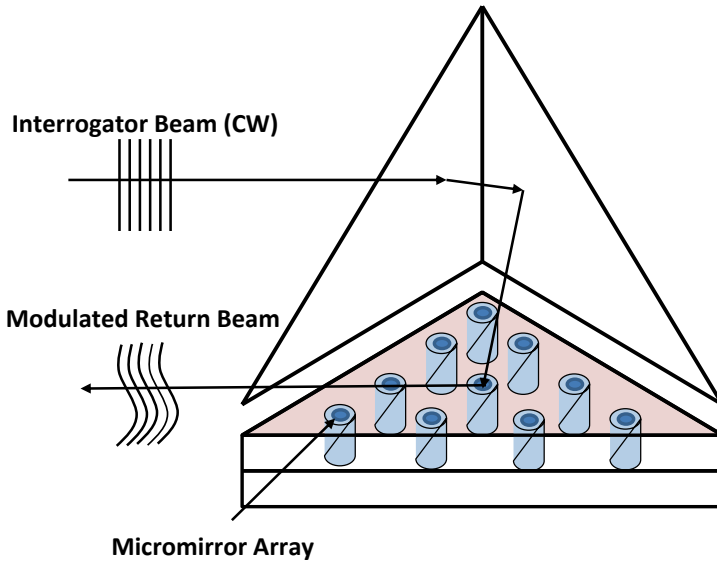
Interrogator Beam (CW)

Modulated Return Beam

Micromirror Array

Fig. 8.9 Concept of modulating retroreflector using MEMS deformable micromirror array (*Reprinted with permission from IEEE, 2006* [18])*. MEMS* micro-electromechanical-system

ing has been considered [20] and also discussed in the earlier section. For a wide range of FSO communications applications, the existing MRR devices are unable to meet all of the requirements such as speed, wavelength, large angular field of view, lightweight, size, power consumption, modulation ratio, operational communication range, etc. Many of these issues have been mentioned in the earlier section. Furthermore for the MRR-based device for FSO communication applications, the system has to operate under varying environmental conditions e.g., turbulence, scattering and maritime atmospheres.

Large-aperture MEMS etalons modulator using a drumhead structure with a variable air gap for use with Cat's-eye retroreflector optics, is reported [21]. Concepts of modified version of similar MEMS device structure to act as a first-surface deformable mirrors rather than an etalon is described in [22, 23]. The first-surface MEMS deformable mirrors are switched from a flat to a hexagonal array of concave micro-lenses. The light distribution due to the spherical micro-lenses are determined by geometrical curvatures (geometrical regime), and interference between multiple diverging beams suppresses the zero-order reflectivity (diffraction effect). The general concept of this type of MEMS deformable mirror for retro-modulator is shown in Fig. 8.9. Note that the far-field diffraction pattern (observed at the receiver plane located near the interrogator laser beam) is the Fourier transform of the deformable-mirror surface (mirror-array). The zero-order diffraction beam determines the signal power collected by the receiver for the FSO communication, located next to the interrogator laser beam. The researchers reported in [23] that they have achieved the following performance: a10-dB contrast ratio for incident

angles upto $\pm 68°$ at 1.5 μm employing three mirrors in a corner-cube retroreflector, each oriented at 54.7° to the normal of the corner-cube, for propagation distances of at least 1 km, with increased drive voltage (≈ 79 V) to increase the devise response to above potential 1 MHz, to be operated hot 20 C and at 100 C temperature, and extinction ratio 7:1.

Micro-Opto-Electro-Mechanical System (MOEMS) Modulator Some types of MEMS-based modulator technology utilize the concept of interference between MEMS micro-mirrors and their support substrate to modulate incident light [24, 25]. The modulating device operates over a large spectral band of wavelengths greater than 1.3 microns and a wide angular range (120°). The modulator consists of an array of silicon micro-mirrors which are parallel to the substrate and suspended by micro-beams above the substrate. The micro-mirrors move coherently and act as interference switch. The modulation is achieved by tuning a large array of Fabry-Perot cavities by applying an electrostatic force to adjust the gap between a movable mirror and the underlying silicon substrate. The basic concept of the modulating device is as follows: The modulator transmission can be modeled as a Fabry-Perot etalon where the mirror reflectivity is determined by the Fresnel reflection coefficient of silicon. The transmission of the modulator for a laser interrogator wavelength with angle of incidence, θ, and a spacing δ between the mirror and the substrate is given by [25]

$$T_{mod} = \frac{T^2}{(1-R)^2} \cdot \frac{1}{1 + \frac{4R}{(1-R)^2} \cdot sin^2\left(\frac{\phi}{2}\right)} \ldots\ldots\ldots\ldots \quad (8.23)$$

where

$$\phi = \frac{4\pi}{\lambda}\delta\,cos\theta$$

and

$$R_\perp = \left\{\frac{\left[\left(\sqrt{n^2 - sin^2\theta} - cos\theta\right)^2\right]}{n^2 - 1}\right\}^2$$

$$R_{11} = \left\{\frac{n^2 cos\theta - \sqrt{n^2 - sin^2\theta}}{n^2 cos\theta + \sqrt{n^2 - sin^2\theta}}\right\}^2$$

where T and R are the transmission and reflectivity of the silicon, n is the index of refraction of silicon at wavelength λ ($n = 3.5$), and $R_\perp$ and R_{11} are the Fresnel reflection coefficients for the perpendicular and parallel polarizations, respectively. For a given angle of incidence, a good modulator contrast can be achieved by varying

the gap. With a high transmission, for a specific gap, the light passes through the retroreflector where the second pass returns to the interrogator. On the other hand, if the transmission is low for the specific gap, the incident light is reflected away at some random angle. The device has to be able to switch between maximum and minimum transmission by changing the spacing of the etalon to values in the range 0.1 to 1.5 microns depending on angle of incidence, θ. An electro-static force determined by the applied voltage between the substrate and the micro-mirrors pull the mirrors down to change the spacing. This type of interference-based MEMS optical modulator using as an interference switch can be used to communicate over a range of 1 km with a bit rate of 200 kbit/s.

MEMS Switchable Retroreflector Film Modulator There are some applications which require signals to be visible and obvious to naked eye. Some of the ideal requirements for these types of applications are: wide visible spectral range for a bright reflection (full width half maximum, FWHM) of > 100 nm, modulation contrast ratio > 10:1, large reflective area (e.g., > 100 cm^2), be able to accept wide input angle, switching at speeds as fast as the human eye response (< 100 ms) for obvious recognition high optical efficiency (i.e., the received retroreflected brightness is much greater than the intensity of reflections from diffusely reflecting surroundings). Low modulation power is also another important consideration. Examples of several electrically modulated retroreflector film technologies for rapid visual identification are introduced in reference [26]. This type of application will be useful for FSO visual communications where a quick response that is obvious to the naked eye is required. This section discusses the interesting switching technology based on electrowetting. The most appropriate modulation technique described here is based on electrowetting which can switch quickly, can modulate over the entire visible spectrum and into the IR, and has little angular dependence. The basic mechanism of electrowetting is the use of electromechanical force to reduce liquid contact angle on a dielectric surface. When a voltage V is applied, the contact angle θ_v can be expressed as [26, 27]:

$$\cos\theta_v = \cos\theta_y + CV^2/2\gamma_{cI} \ldots\ldots\ldots\ldots\ldots \quad (8.24)$$

Where θ_y is Young's angle (with no voltage applied), C is the capacitance per unit area of the hydrophobic surface (F/m^2), and γ_{cI} is the interfacial surface tension (*N/m*) between conducting fluid (e.g., water) and insulating fluid (e.g., oil). The polar fluid serves as one electrode. Electrowetting can be applied to change optical transmission with a speed as fast as a few ms for devices of < 100 μm in size applying 10–100 V voltage depending on the properties of the materials such as C and γ_{cI}.

The incident light must transmit through the modulation layer, retroreflect, and then pass back through the modulation layer a second time. Reference [27] describes switchable retroreflectors based on electrowetting lenslets that are integrated into the corner cubes. Figure 8.10 illustrates the basic principle. A corner cube retroreflector backplane is coated with electrowetting films and dosed with oil ($n > 1.4$) and water ($n \approx 1.3$). The oil and water creates a concave-shaped meniscus and acts
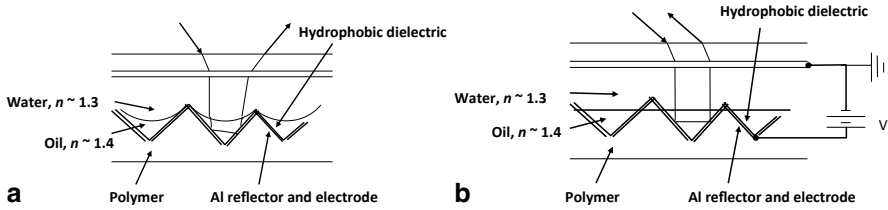
Fig. 8.10 Electrowetting lenslet retroreflector modulation. **a** Scattering state (voltage off). **b** Retroreflection (voltage on) (*Reprinted with permissionfrom the Optical Society of America (OSA), 2012* [26])

like a concave lens since the refractive index of oil is higher than that of water. The researchers have used 800 μm corner cubes when the voltage is off ($V=0$), the light incident onto the electrowetting retroreflector will be refracted passing through the concave meniscus and thus be optically scattered. The device then works like a diffuse reflector. When the voltage V is applied, electrowetting reduces the water contact angle with hydrophobic dielectric. Applying voltage ≈ 19 V, the water contact angle reaches $\approx 125°$, the meniscus becomes flat and the device behaves like a conventional retro reflector. A contrast ratio of greater than 10:1 was achieved with input angle $\pm 30°$. If the corner cube is scaled to 10 μm, a very fast switching speeds of <0.1 ms can be reached (far exceeds the response time of the human eye). Also, a large total reflective area ($\approx > 100$ cm^2) can be fabricated which can be thin and flexible (i.e., can be put on curved surface directly).

8.4.6   Fiber-based Amplified-Retro-Modulator (ARM): A New Concept in MRR Technology Amplified Retro-Modulator (ARM) based on single-mode optical fiber (SMF)

a. *Single channel ARM*

The performance of the laser communications return link in a MRR system is limited by the size (area) of the retro-modulator. A larger aperture retro-modulators can return more signal, but is much heavier and consume more electric power. A new concept of MRR is described in the reference [28] which uses an amplifying retro-modulator. The amplifier increases the effective area of the retro-modulator more than 300 times to make the system as effective as a larger aperture passive retro-modulator without the increased weight and power consumption of a larger retro-modulator.

How does it work? The concept is based on developing a high-efficiency FSO-SMF coupler. The conventional couplers suffer high losses. The FSO receiving element is a single-mode fiber fused to the end of a solid optic with a demonstrated increase in efficiency and achieving a very high data rate of 2.5 Gbps with this

type of retro-modulator [28]. With the conventional FSO systems for coupling into single-mode fibers, the depth-of-focus (DOF) is very small and for an ideal imaging system is given by:

$$DOF = \frac{d}{2.NA}$$ (8.25)

where d is the focal spot and NA is the numerical aperture of the optical fiber. For conventional single-mode fiber with a mode-field-diameter of 10.5 µm and the NA of 0.13, the DOF is 40 µm. There is therefore a severe coupling efficiency losses because of a small change in the position of the lenses due to thermal expansion or any mechanical vibrations. The new concept utilizes the pigtailed solid glass fiber collimators which are less sensitive to thermal and mechanical disturbances since the optical fiber is fused directly to the glass of the collimator. For efficient coupling of light into a SMF the light at the entrance of the receiver must have an étendue that does not exceed the étendue of the SMF and is constrained by the upper limit on the V parameter for a SMF [29]:

$$V = \frac{2\pi a_{core}}{\lambda} \cdot NA = \frac{2\pi a_{core}}{\lambda} \cdot \sin(\theta) \le 2.405$$ (8.26)

where a_{core} represents the radius of the fiber core, λ is the operating wavelength, θ is the acceptance angle of the fiber. The étendue of a single-mode fiber is given by:

$$\xi_{SMF} = \pi \cdot (a_{core} \cdot NA)^2 \le \frac{(1.2025 \cdot \lambda)^2}{\pi}$$ (8.27)

where ξ_{SMF} represents the étendue of a single-mode fiber. For efficient coupling, the receiver étendue, $\xi_{receiver}$, must not exceed the étendue ξ_{SMF} of the single-mode fiber. The theoretical FOV of coupling a 2-cm diameter optical beam into an optical fiber would be 68-µradians or 14-arcsec, although in the reference [28] the experimental value of the FOV was very low, 0.8-arcsec which could be increased with the proper design of the lens system.

It was pointed out in the reference [28] that a high-efficiency optical coupling of FSO signals into a single-mode fiber was possible by combining high efficiency FSO-SMF optical couplers with high-speed modulators and very low-power consumption Erbium Doped Fiber Amplifiers (EDFAs). It was possible to develop an ARM with a return signal 2000 times the return signal from an identical aperture conventional MRR that can simultaneously be operated at several Gbps modulation rates. The total power consumption of an amplified 2.5-Gbps ARM used only 120-mW of electrical power.

The intensity incident upon a typical MRR is given by:

$$I_{inc} = \frac{P_T \cdot \eta_T \cdot \eta_{Atm}}{\Omega_T \cdot R^2}$$ (8.28)
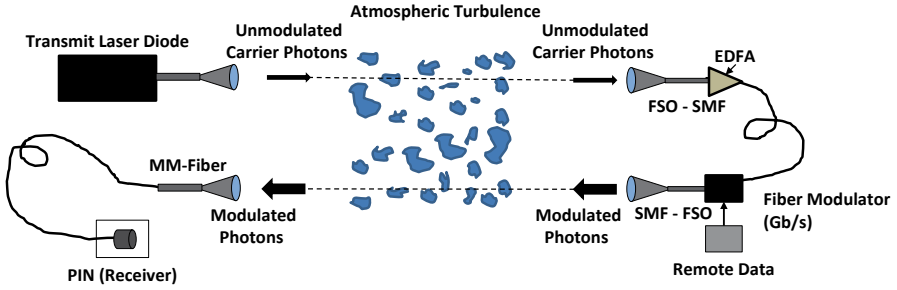
Fig. 8.11 Single-fiber-based Amplified Retro Modulator (ARM) (*Reprinted with permission from Thomas Shay/SPIE, 2004* [28])

where P_T is the transmitted power, η_T represents the efficiency of the transmit optics, η_{Atm} is the atmospheric transmission efficiency, Ω_T represents the divergence of the transmitted beam, and R represents the link range. The return signal for a conventional MRR is given by [30]:

$$P_S = I_{inc} \cdot A_{eff\_retro} \cdot \eta_{receiver} \cdot \eta_{Atm} \cdot \frac{A_{receiver}}{\Omega_r \cdot R^2} = \frac{P_T \cdot \eta_T \cdot \eta^2_{ATm} \cdot \eta_{receiver} \cdot A_{receiver}}{\Omega_T \cdot \Omega_r \cdot R^4} \cdot A_{eff\_retro} \quad (8.29)$$

where A_{eff_retro} is the effective area of the retro-modulator, $A_{receiver}$ is the receiver area, Ω_r is the divergence of the retroreflected beam, λ is the interrogator laser wavelength. If the retro-modulator has a gain of G, then the effective area of the retro-modulator is given by:

$$A_{eff\_retro} = G \cdot A_{retro} \quad (8.30)$$

where A_{retro} represents the physical area of the retro-modulator. From the above equations, the return signal from an ARM with a gain G is obtained as follows [28]:

$$P_s = \frac{P_T \cdot \eta_T \cdot \eta^2_{ATm} \cdot \eta_{receiver} \cdot A_{receiver}}{\Omega_T \cdot \Omega_r \cdot R^4} \cdot A_{retro} \cdot G \quad (8.31)$$

The above equation clearly shows that the return signal from an ARM with a gain G increases the received signal by a factor G compared with a MRR with the same aperture. With commercially available EDFA systems with a 40-dB small signal gain, it is possible to increase the effective area of the retro-modulator by nearly 4 orders of magnitude [28]. The effect of the spontaneous emission noise on the receiver SNR can be neglected. Figure 8.11 shows a schematic block diagram of the ARM system which can operate under atmospheric turbulence condition. Unmodulated photons from the interrogating diode laser beam (SMF pigtailed/collimated) are collected by the ARM's receive aperture, and coupled into a SMF (pigtailed). This method provides a robust high efficient coupling from free-space into a SMF. After amplification (using EDFA) and then subsequently the modulation, the outgoing

photons exit the smaller aperture fiber pigtailed collimator, which is co-aligned with the receive aperture at the interrogator laser location. The amplified and modulated beam thus is retroreflected back to the source and collected by a receive optics. The first retro-modulator operating at 2.5 Gbps was demonstrated in the laboratory [28].

b. *Fiber-Array-based (Multiple Channel) ARM*

The ARM described above is limited to its extremely small FOV of about $\pm 0.004°$ only. In order to overcome this limitation, a recent patent by the author and his colleague [31] (Patent No. US 8, 301, 032 B2, Oct. 30, 2012) describes a wide FOV amplified Fiber-Retro system. The concept is to provide a pixellated fiber array system for both incoming and outgoing optical beams to maintaining one-to-one correlation between each set of lenslet/fiber array which can also determine the exact location of the source. The patent describes a means of achieving a wide FOV "fiber retro" system where the remote device can accept a wide angle of interrogating signal. The system consists of the receiving optics, the $N \times 1$ combiner in combination with the fiber tap, and the probe photodetector, the electronic $N \times 1$ switch, the $1 \times N$ spatial router, and the single-mode optical amplifier. Figure 8.12 shows the diagram of the "fiber retro" system. The system includes all-optical repeater without optical-to-electrical-optical (OEO) conversion process. The combined wide-angle lens and the lenslets/SMF pigtailed collimator provide the needed requirements for coupling the incident light onto the lenslets array. A wide-angle telecentric lens is incorporated with an array of the single element FSO-SMF couplers. The incident signal photons enter the telecentric lens, imaged onto the lenslet array; the output signal (after the combiner) is then optically amplified in a low-noise highly efficient EDFA. Next the signal is modulated in an electro-optical intensity modulator according to the external data. Finally the modulated and amplified photons sent out the exit port (transmit optics) back to the interrogator laser (transmitter) location. If the entrance and exit apertures are aligned to produce parallel beams, then this configuration serves as an amplified retroreflector/retro-modulator.

Effects of atmospheric turbulence on the amplified fiber retro-modulator (AFRM) The effect of atmospheric turbulence on the AFRM system using an array of fiber couplers needs to be evaluated. This can be best understood by estimating the variance of angle-of-arrival fluctuations caused by the presence of atmospheric turbulence which can be written as:

$$\sigma_a^{\ 2} = 2.914 D^{-1/3} H^{-5/3} \int_0^H z^{5/3} C_n^{\ 2}(z) dz \qquad (8.32)$$

where D=aperture diameter, $C_n^{\ 2}$ is the turbulence strength, and H is the altitude. If the communication link is along a slant path, then $C_n^{\ 2}(z)$ should be replaced by $\sec(\theta)$. $C_n^{\ 2}(z)$ where θ is the zenith angle (away from the vertical) and the limit of integration should be taken as the slant range.

An example of link analysis for a Satellite-based system laser interrogator and low-power Gbps amplified fiber retro-modulator Figure 8.13 shows the simulation
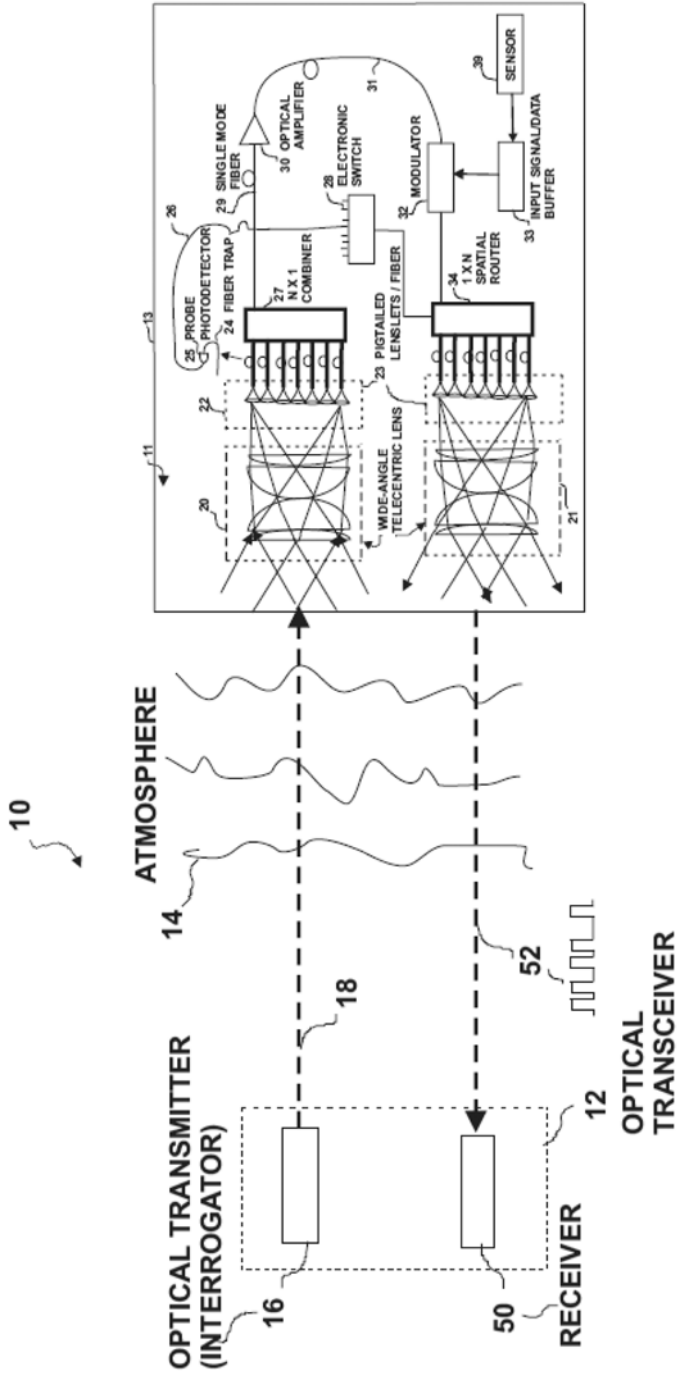
Fig. 8.12 Fiber-array-based wide-field-of-view Amplified Retro Modulator
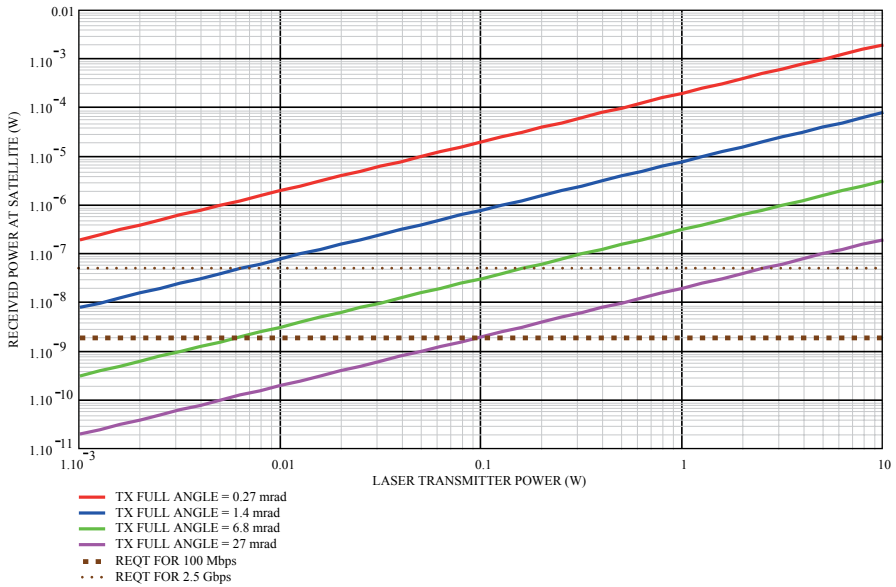
Fig. 8.13 Plot of the received power versus required laser transmitter power: an example of a Satellite-based laser interrogator and a ground-based "Fiber retro" system using fiber-array

result for a satellite-based laser interrogator and ground-based ARM. The range of the satellite was assumed to be 370 km the atmospheric transmission efficiency $=0.5$. The retroreflected beam is received by the satellite receiver of 6 in. diameter. The transmitter efficiency was assumed to be 0.5, the required bit-error-rate (BER) $=10^{-9}$, the SNR $=144$, and the gain of the retro-modulator system was taken to be 4×10^5. The simulation result shows the received power at satellite as a function of required laser transmitter power on the satellite for different values of the divergent angles of the transmitter. The two horizontal dashed lines represent the needed received power at the satellite for 100 Mbps and 2.5-Gbps data rates. To achieve a data rate of 2.5-Gbps, for a transmitter divergent beam of 6.8 mrad, it requires 160 mW of laser power whereas for transmitter divergent beam of 27 mrad, it requires about 2.5 W of laser power. These numbers are very practical and realistic.

Comparison of different MRR technologies A comparison of the features of various MRR technologies discussed in this section is summarized in Table 8.1.

8.5   MRR-based FSO Communications Systems Performance Analysis

This section will discuss the following: first, a link budget analysis for evaluating received power at the transceiver; second, determine SNR for MRR communication system; third, calculate BER for a MRR FSO communication system in presence of

Table 8.1 Performance characteristics of different MRR technology

MRR technology	Liquid crystal (LC)/Ferro-electric liquid crystal (FLC)	MQW	Electro-optics	MEMS	Amplified fiber-retro: single chan-nel/fiber array
Modulation	Polariza-tion and amplitude	Amplitude	Polariza-tion and amplitude	Amplitude	Amplitude
Speed	Slow	Medium-fast	Fast	Low/medium	Very fast possible
Power consumption	Very low	Medium	High	Low	Very low
Voltage required	Low	Low	High	Low/moderate	N/A (does not require any electro-optical. acousto-optical, LC or MQW material)
MRR diameter	Large	Medium	Medium	Small	Very small for single chan-nel to small for array device
Mass	Low	Low	High	Low	Very low
Comments		Simple and rugged, easy to array for wide FOV; response shifts with temperature Cat's eye is capable of higher bandwidth	AOM can be very com-pact and high-speed possible	Low cost; deformable micro-mirror array possible for higher modulation contrast, and larger FOV	Single chan-nel has extremely small FOV; array of fiber retro provides large FOV

MRR modulated retroreflector, *MQW* multiple quantum well, *MEMS* micro-electromechanical modulators system, *AOM* acousto-optic modulators

atmospheric turbulence; finally, atmospheric scattering effects in the retroreflected received signal power will also be discussed.

8.5.1   Link Budget Analysis

MRR Link Scenario In order to establish an MRR FSO communication link, the interrogator laser would illuminate the MRR-equipped terminal. Small photodetectors or the modulator itself would be able to detect the incident beam and cue the

data transmission. If the retroreflected return beam is amplitude modulated, HDX communications are possible. This can be done simply with an OOK modulation, but more advanced modulation schemes such as pulse position modulation (PPM) can be used for higher data rates. For FDX scheme such as polarization modulation, for example, can be utilized on the interrogation uplink, and amplitude modulation (OOK) can be used for return data format in MRR down link. A receiver telescope would be co-located with the interrogator and would be equipped with the necessary optics, detectors and electronics to decode the received data stream.

Link Budget Calculations MRR system consists of three main components: MRR device, the data compressor, and the data system. The MRR makes the bidirectional nature of a typical communication link into a one-sided alignment problem. A retroreflective communication system thus comprises a laser transmitter/receiver station and a remote retroreflector that can be switched "on" or "off" states. The link budget is the computations of the optical power losses in one link and is bounded by the system dynamic range given by the transmitter output power and the receiver sensitivity. After subtracting all the optical losses across the link, any remaining dynamic range is referred to the "Link Margin", allows a link to operate under adverse atmospheric condition. There are basically three retroreflector losses: absorption loss, wave front loss (due to imperfection of the retroreflective optics), and contrast ratio (for example loss due to a certain percentage modulation depth of the quantum-well modulator).

Limitations with MRR FSO Communications All FSO communications experience limitations imposed by the atmosphere, e. g. weather-dependent attenuation. Furthermore, atmospheric turbulence causes beam spreading and wandering as well random fluctuations of the received communication signal (scintillation). While atmospheric attenuation causes large but slowly varying SNR at the receiver, turbulence causes fast SNR fluctuations (i. e., fading). In heavy fog the attenuation can be as large as 80 dB/km, or more, while in some other conditions, it may be only a few dB/km. Because of scintillation and beam wandering, turbulence reduces the received signal energy in the detector. Atmosphere therefore limits the performance of FSO communications systems, and plays an important role in the link budget analysis discussed below. In order to implement an MRR-based FSO communication, atmospheric effects such as turbulence and scattering must be considered. For example, backscatter from the interrogating beam where photons scattered by the atmosphere reflect back into the optical receiver's optical path and reduce the SNR. Mitigation techniques to reduce turbulence and scattering effects on MRR-based FSO communication system need to be employed to accomplish acceptable BER required by the FSO system.

8.5.2   *Quantifying the Link Budget*

The MRR acts both as a receiver and a transmitter in the optical link, the MRR optical link budget can be expressed in terms of gains and losses. To estimate the range for the MRR communication link the reflected optical power reaching the

transceiver must be estimated. In terms of gains and losses, the MRR optical link budget can be expressed as follows [12, 17]:

$$P_{rec} = P_{laser} G_{Tx} L_{Tx} L_R T_{atm} G_{MRR} L_{MRR} M L_R T_{atm} G_{Rx} L_{Rx} \tag{8.33}$$

where:

P_{rec} = received signal power
P_{laser} = interrogator laser power
G_{Tx} = transmitter antenna gain (laser collimation and pointing)
L_{Tx} = transmitter losses
L_R = range losses due to propagation path
T_{atm} = atmospheric transmission = $e^{-\alpha R}$, where α is the atmospheric coefficient of attenuation
G_{MRR} = MRR antenna gain = $\left[\dfrac{\pi D_{retro}}{\lambda}\right]^4 S$ (where D_{retro} = optical aperture of the retroreflector, i.e., MRR diameter, λ is the interrogator laser wavelength, and S is the MRR Strehl ratio of the optic [2]: some typical value of a MQW retro-modulator, $S = 0.4$)
L_{MRR} = MRR optical losses
M = MRR modulation efficiency
G_{Rx} = receiver antenna gain (due to interrogator receive aperture)
L_{Rx} = receiver losses

Some of the terms in the above link budgets equation can be calculated from the following formulas:

$$G_{Tx} = \frac{32}{\theta_{div}^2}, \text{ where } \theta_{div} = \text{transmitter divergence } (1/e^2 \text{ full})$$

$$L_R = \left[\frac{\lambda}{4\pi R}\right]^2, \text{ where } R = \text{range}$$

$$G_{Rx} = \left[\frac{\pi D_{Rx}}{\lambda}\right]^2, \text{ where } D_{Rx} = \text{receiver diameter}$$

Note the strongest dependence of retroreflector links on the range which falls off as fourth power; the links fall off more strongly with range than conventional links because of their bi-directional (double-pass) nature. Due to this R^{-4} dependence, compared to the R^{-2} dependence for a one-way conventional free-space communication link, it therefore requires appreciably more to change communication performance. For example, to increase the communication range by a factor of ten, it will require four orders of magnitude in optical power. Also, the optical power received depends on the retroreflector diameter as fourth power. For MRR systems, a large aperture to minimize the transmission losses and a high modulating rate are desired at the same time. But the modulator switching time is usually RC-limited and therefore gener-

ally inversely proportional to the size of the modulator's active surface area. Thus a large retroreflector aperture will slow down the data rate and a trade-off is needed for determining the aperture size to maximize the returned optical power and the required high speed data rate while keeping the consumed electric power low. For terrestrial applications, the atmospheric losses are caused due to absorption and scattering such as Rayleigh and aerosol scattering. Propagation effects are different at different wavelengths and therefore the interrogator laser wavelength needs to be chosen accordingly. Finally, atmospheric turbulence will cause large and rapid SNR fluctuations in the received optical power (fading on a millisecond scale).

From the above link equation, the received power can be predicted for a given system architecture. For a given data rate and encoding scheme of the modulating element the number of photons received by the detector, per transmission bit can be calculated as follows:

$$n_p = \frac{Q \cdot P_{rec}}{h\nu R}$$

(8.34)

where:
n_p = photons per bit
Q = quantum efficiency of the detector
h = Planck's constant (6.63×10^{-34} Js)
ν = frequency of light = c/λ
R = data rate

8.5.3   BER Calculation for MRR System in Presence Atmospheric Turbulence

Understanding the contribution of scintillation to the power fluctuations due to atmospheric turbulence is essential to improving the performance of FSO communication systems. BER is the standard figure-of-merit for a communication link. A BER of 10^{-6} is generally considered to be acceptable. BER is inherently limited by the contrast ratio of the modulating retroreflector device. When the signal received is very low, i.e., at the low photon levels characteristics of a communication link, the BER will be determined by the signal level, the noise in the detector and the contrast ratio of the retro-modulator device. A combination of techniques such as compression techniques, signal processed, and appropriate adaptive optics-based techniques would be necessary to improve the BER in a MRR-based FSO communication system.

Atmospheric turbulence causes the interrogator beam and the reflected beam to spread reducing the average signal level, and secondly it induces spatially and temporally varying fluctuations in intensity (scintillation). Scintillation causes the received signal to fluctuate above and below the accepted mean value, when bits of transmitted data may be lost whenever the signal is low. The signal strength

and the probability of wrongfully identifying the logic state of the signal assumes that there is an identifiable threshold signal value which separates logic state 1 (presence of signal) from logic state 0 (no signal). However, this optimal threshold value for a given bit varies with time in presence of atmospheric turbulence (due to scintillation effect). In this case, a variable threshold that is always optimal can still be implemented provided the turbulence-induced temporal fluctuations are much slower than the bit rate.

System Model for MRR-based FSO Communication in Presence of Atmospheric Turbulence

Similar to the link equation above, the signal power received by the interrogator-receiver from the MRR is given by [32]:

$$P_{rec} = \left\{ \frac{16 T_{atm}^2}{\pi^2 R^4} \frac{P_{laser}}{\theta_{div}^2} \frac{A_{rec}}{f_{rec}} \frac{\sigma_{MRR}}{C_{logic}} \right\} \cdot \frac{1}{W_{EO}^2} \frac{1}{W_{ER}^2} \cdot (T_1 \cdot T_2)$$

$$= \frac{G_R G_{sys}}{R^4} \cdot \frac{1}{W_{EO}^2} \cdot \frac{1}{W_{ER}^2} \cdot (T_1 \cdot T_2) \qquad (8.35)$$

The first bracketed term $\{..\}$ can be written as $G_R G_{sys}/R^4$ which is the power received from the MRR with no turbulence. The other terms contribute to the received power in presence of turbulence. In the above equation, T_{atm} is the atmospheric transmission, θ_{div} is the transmitter divergence, and f_{rec} is the collection efficiency of receiver optic. The MRR is characterized by a cross-section σ_{MRR} and contrast C_{MRR}, where C_{MRR} is the "on/off" contrast ratio between logic 1 and logic 0. The power received for logic 1 from the above equation can be calculated by writing $C_{logic} = 1$, and for logic 0, the power is determined by writing $C_{logic} = C_{MRR}$. The parameter G_R was used which deviates from 1 to identify how the system performs for some deviations from a given system configuration defined by G_{sys} (e.g., due to change in orientation or angle of incidence). The term $1/(W_{EO}^2 W_{ER}^2)$ is the reduction in mean power due beam spreading on the outgoing (from interrogator to MRR) and return (from MRR to interrogator) paths. The terms T_1 and T_2 denote time-varying (due to scintillation) transmission in the outward and return paths. For a pulsed interrogator with a repetition frequency f_{rep}, the mean received energy per pulse is given by $E_{rec} = P_{rec}/f_{rep}$.

Effects of Atmospheric Turbulence on MRR-based FSO Communications

To understand the MRR-based FSO communications system which has to operate under atmospheric turbulence, the following factors need to be taken into account:

1. Received power fluctuations of the interrogator laser beam after propagating through a range, R under atmospheric turbulence characterizing by the refractive index structure constant C_n^2, an inner scale l_0, and an outer scale L_0. For horizontal path, C_n^2 is typically from 10^{-12} m$^{-2/3}$ to 10^{-16} m$^{-2/3}$, l_0 is about 2–10 mm, and L_0 is on the order of the distance between the optical path and the ground. This is usually specified as the Rytov variance, σ_1^2 which is given by [33]:

$$\sigma_1^2 = 1.23 \, C_n^2 k^{7/6} R^{11/6} \tag{8.36}$$

where k is the wave number, $k = 2\pi/\lambda$ for the interrogator wavelength λ.

2. The change in beam diameter term for the beam propagating from the interrogator to the MRR, denoted by W_{EO} in the earlier equation of the received power and is given by $W_{EO} = W_e/W$, where W is the beam diameter in the absence of turbulence. W_e can be calculated [33] from the equation:

$$W_e = W \left(1 + 1.33 \, \sigma_1^2 \Lambda^{\frac{5}{6}} \right)^{1/2} \tag{8.37}$$

where $\Lambda = \dfrac{2R}{kW^2}$

3. The change in the beam diameter, W_{ER} for the beam reflected from the MRR reaching to the receiver location: In this case, the beam starts from the MRR aperture propagates towards the interrogator at which point the beam diameter is changed due to the effect of atmospheric turbulence.

4. Probability density function (PDF) of intensity fluctuations of laser beam—single and double passage:

Single passage PDF The statistics of the intensity fluctuations propagated through atmospheric turbulence is characterized by PDF, one of the recently accepted forms is given by [33] which is a Gamma-Gamma PDF:

$$p(I) = \frac{2(\alpha\beta)^{\frac{\alpha+\beta}{2}}}{\Gamma(\alpha)\Gamma(\beta)} I^{\frac{\alpha+\beta}{2}-1} K_{\alpha-\beta}\left(2\sqrt{\alpha\beta I}\right) \tag{8.38}$$

where I is the intensity normalized to the mean value, α *and* β are parameters related to scintillation, $K_\nu(x)$ is a modified Bessel function of the second kind, $\Gamma(x)$ is the gamma function. For a given scintillation index, the values of α and β can be calculated [33].

Double passage PDF The beam first originates from the interrogator laser transmitting a power P_0 producing a power P_1 at the MRR aperture, and the resultant reflection power is P_2 through the receiver aperture. The transmission parameters T_1 (from the interrogator to the MRR) and T_2 (from the MRR back to the interrogator) in the MRR received power equation discussed earlier, are time varying and fluctu-
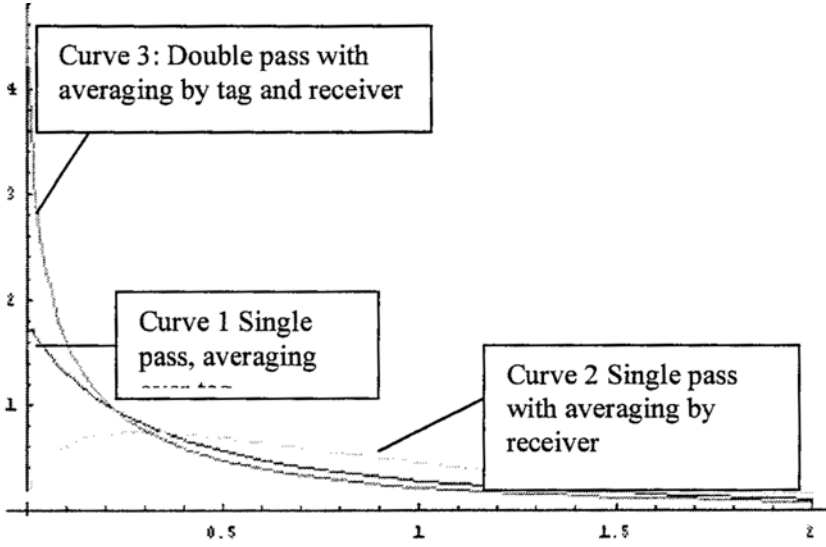
Fig. 8.14 Double-pass PDF of transmission for modulating retroreflector in presence of atmo-spheric turbulence: single-pass PDF's of transmission are also shown for comparison (*Reprinted with permission from SPIE, 2004* [32]). *PDF* probability density function

ates according to the turbulence characteristics of the atmosphere. The mean value of the effective transmission in each direction is 1. These transmissions in each direction can be uncorrelated so that the joint PDF can be written as the product of the individual PDFs. The double passage PDF can then be written as [32]:

$$T = T_1 T_2, \ and \ therefore \ dT_2 = dT/T_1 \qquad (8.39)$$
$$P(T_1, T_2) = P_1(T_1) \, P_2(T_2)$$

One can then obtain the PDF of total round trip transmission:

$$P(T)dT = \int P_1(T_1) \, P_2\left(\frac{T}{T_1}\right)\frac{dT_1}{T_1} dT \qquad (8.40)$$

The double passage PDF can therefore be computed from the individual PDFs in each direction. Figure 8.14 shows the double pass PDF of transmission for MRR communication scenario. The single passage PDF with aperture averaging for MRR aperture and receiver telescope aperture are also shown in the figure. From the figure, it is clear that even with aperture averaging (to reduce the fluctuations due to scintillation) a double passage propagation can lead to a high level of fluctuations with a high probability of low power at the receiver. The MRR-based communication link design should take into this effect in order to determine the various system

parameters (such as aperture size for different turbulence levels, power levels of interrogator laser etc.).

BER Calculation for MRR System

In order to determine the BER of the MRR FSO communication system, one needs to know the basics of received signal, contributions of all noise sources in the system, and the relationship between the SNR to communications system performance defined by BER. A general discussion and relationship of received SNR and BER can be found in references [34, 35]. In almost every area of measurements, the ultimate limit to the detectability of a weak signal is set by noise-unwanted signals that obscure the desired signal. For laser communications systems the shot noise, background noise and thermal noise contribute to the total noise at the receiver. The goal of a lasercom system for digital communication is to transmit the maximum number of bits per second over the maximum possible range with the fewest errors. Electrical data signals are converted to optical signals via a modulator. A "1" is transmitted as a pulse of light while a "0" has no light output. The number of "1's" and "0's" transmitted per second determines the speed of the link (bit rate). At the receiving end of the link, the optical signal is detected by an optical-to-electrical converter (e.g., a photo detector). A decision circuit then identifies the "1's" and "0's" in the signal, and thus recovers the information sent. For an OOK modulation, for example, decoding is based on a decision as to whether the pulse slot time has high enough field energy or not. The selected threshold determines the best performance in decoding the correct signal with the lowest probability of making a bit decision error and thus the BER can be obtained. Thus the performance of the lasercom system can be predicted by computing the BER of the system which depends on the modulation format, and the SNR. The noise comes from all possible sources which include shot noise, dark current noise, thermal/Johnson noise in the electronics following the photodetector, and the background noise.

The calculation of BER for MRR system thus involves three steps: (i) compute the SNR for the detector (no turbulence), (ii) calculate the BER using mean signal energy and a threshold value of the signal(no turbulence), (iii) finally, calculate BER for the fluctuating signal due to turbulence (i.e., with turbulence). The procedure is discussed a follows.

1. SNR at the receiver aperture using an avalanche photodetector (APD) as an example:

The shot noise current for an APD is given by [32]:

$$I_{noise-Det} = \sqrt{2eB(I_{surf} + (I_{sig} + I_{bulk} + I_{bkgr})M^{2+\varepsilon}) + I_{amp}^2} \qquad (8.41)$$

where e is the charge of the electron, B is the bandwidth of the system, and I_{surf}, I_{sig}, I_{bulk}, I_{bkgr}, I_{amp} are respectively the surface dark current, signal current (as a result of received signal power, P_s), the bulk dark current, a background

current (originating from background power, P_{bkgr}), the noise current due to the signal fed into a preamplifier, and M is the gain of APD in the operating mode. The unit of all the currents is ampere, ε is the excess noise factor for the detector. The SNR is then given by:

$$SNR_{Det} = \frac{\eta P_s}{I_{noise-Det}} \tag{8.42}$$

where the detector efficiency parameter, $\eta = MR$ and R is the detector responsivity (A/W).

2. The BER using mean signal energy and a threshold value of the signal (no turbulence):

Assuming the noise of the detector is Gaussian, the probability distribution of the received signal S, with a mean value of S_{mean} and signal variance σ_s^2 can be written as

$$P(S) = \frac{1}{\sigma_s \sqrt{2\pi}} exp\left\{ -\frac{(S - S_{mean})^2}{2\sigma_s^2} \right\} \tag{8.43}$$

The distribution functions for logic 1 and logic 0 signals will be different. Consider a string of pulses where fluctuations are due to shot noise only For logic states 1 and 0, the mean signals S_1 and S_0 are given by $S_1 = RE_{mean}$ and $S_0 = RE_{mean}/C_{MRR}$, respectively, and the corresponding noise components $N_1 = NE_{mean}$ and $N_0 = N(RE_{mean}/C_{MRR})$, respectively. Note that E_{mean} is the mean energy per pulse received by the receiver and C_{MRR} is contrast between the mean signal for logic state 1 and that for logic state 0. Assuming the probability of false alarm equals the probability of missed detection, i.e., the probability of wrongfully detecting logic 1 is the same as the probability of wrongfully detecting 0, the threshold signal, S_{th} can be found as

$$S_{th} = \frac{(\sigma_0 S_1 + \sigma_1 S_0)}{(\sigma_0 + \sigma_1)} \tag{8.44}$$

The BER or the probability of error can then be found from

$$\text{NO TURBULENCE:}\quad BER_0 = \frac{1}{2}\left\{ erfc\left(\frac{S_1 - S_{th}}{\sqrt{2}\sigma_1} \right) + erfc\left(\frac{S_{th} - S_1/C_{MRR}}{\sqrt{2}\sigma_0} \right) \right\} \tag{8.45}$$

where $erfc$ is the complimentary error function.

3. The BER for the fluctuating signal due to turbulence (i.e., with turbulence):

In order to determine the BER in presence of atmospheric turbulence, the BER_0 which is considered as a conditional probability must be averaged over the PDF of the random signal to determine the unconditional mean BER [34, 36]. To perform the calculation the form of the PDF of intensity fluctuations through atmospheric
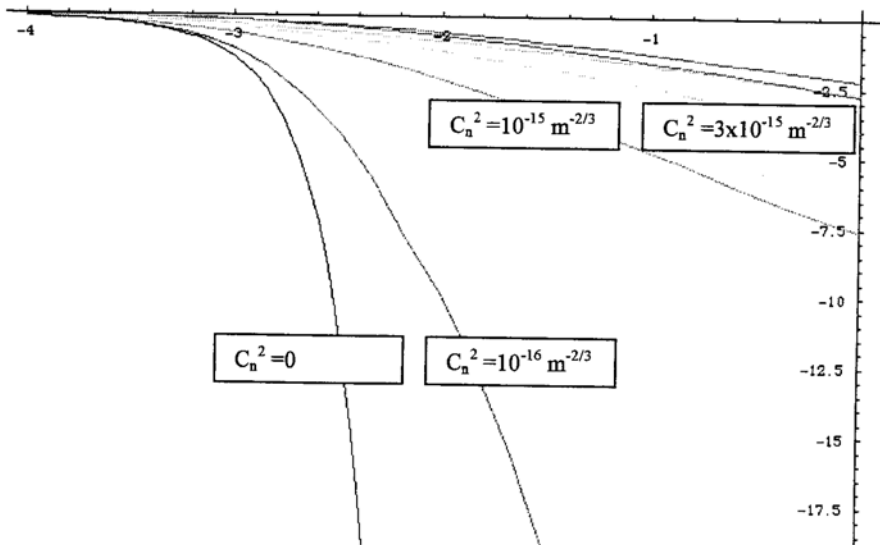
Fig. 8.15 BER (log-scale) versus system parameter G_R (log-scale) for different turbulence strength parameters, C_n^2 (*Reprinted with permission from SPIE, 2004* [32]). *BER* bit-error rate

turbulence is required. A Gamma-Gamma distribution was proposed earlier. The BER for a turbulence-induced fluctuation for a MRR FSO communication link can be written as

$$\text{IN PRESENCE OF TURBULENCE:} \quad BER_{Turb} = \int_0^\infty BER_0(E)p(E)dE \quad (8.46)$$

where BER_0 is the BER associated with a given pulse energy with no turbulence from the earlier equation, $p(E)$ is the PDF for the incoming energy taking into account of the pulse repetition frequency of f_{rep} (note: mean received energy E_{rec} per pulse for a pulsed interrogator with a repetition frequency is related to the received power, P_{rec} by $E_{rec}=P_{rec}/f_{rep}$). A Gamma-Gamma distribution generally valid for weak to strong turbulence regime was mentioned earlier. Figure 8.15 shows a plot of system parameter relative cross-section G_R versus BER in presence of atmospheric turbulence, BER_{Turb} (for various values of turbulence strength parameter, C_n^2). A relative cross section of value of G_R of 0.3 % means the value in the log scale to be $\text{Log}_{10}(G_R)=-2.5$. From the figure, it is clear that for a given system value of G_R, the BER for the MRR system increases as the strength of turbulence becomes stronger and stronger from the no turbulence case ($C_n^2=0$) to $C_n^2=10^{-16}$ m$^{-2/3}$, and then to $C_n^2=10^{-15}$ m$^{-2/3}$. The combination of C_n^2 and the system required BER to be achieved determines the limits of retroreflective communications systems that have to operate under atmospheric turbulence. The BER can be improved by increasing the system parameter $G_R G_{sys}$ which can be accomplished by using a higher interrogator laser power, a larger aperture MRR, or a more efficient collection geometry.
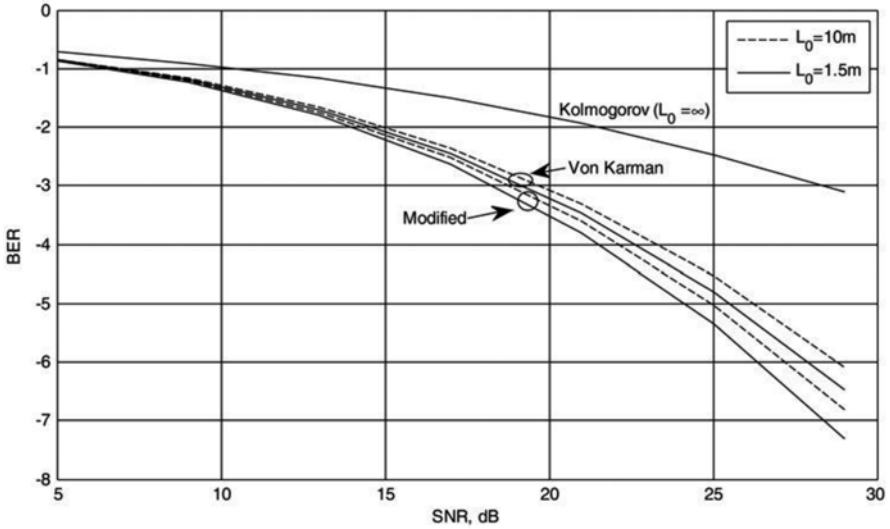
Fig. 8.16 BER (log-scale) versus SNR (dB) for different atmospheric models (spatial spectrums; *Reproduced with permission from IET, 2012* [37]). *BER* bit-error rate, *SNR* signal to noise ratio

A trade-off between all these parameters need to be performed in order determine the optimum MRR-based FSO communications system.

Recent results on the method for the evaluation of performance of free space optical communication systems utilizing MRR under weak turbulence are described in the Ref [37]. Figure 8.16 shows the BER against SNR for various spatial spectrum of atmospheric turbulence models (Kolmogorov, Von Karman, and Modified). The results are valid for weak turbulence where a log normal distribution of PDF was assumed. The results show that different spatial spectrum (i.e., different turbulence models) adopted for the calculations of BER can lead into differences in SNR required for the communications stems design. The performance model for the MRR-based FSO communications systems can be used to evaluate the system performance in terms of BER as a function of SNR, aperture diameter, MRR size, inner and outer scale sizes, C_n^2, and link distance. The model can be used for network design and for network routing with proper algorithms.

8.5.4   Atmospheric Scattering Effects on MRR-FSO Communications System

The previous section deals with the clear air turbulence (CAT) effects on the MRR FSO communications systems performance. This section will discuss the atmospheric scattering effects. There is always scattering when the photons emerging from the interrogator laser beam propagates through atmosphere. The scattering

photons can play an important role among the total photons captured by the receiver and therefore it is important to analyze the influence of atmospheric scattering on an MRR communication link.

The communication channel in this case is atmosphere which consists of air molecules and aerosol particles: the optical parameters of air molecules are the extinction coefficient k_e^{air}, the scattering coefficient k_s^{air}, and the absorption coefficient k_a^{air}, and those of aerosol particles are the extinction coefficient k_e^{aer}, the scattering coefficient k_s^{aer}, and the absorption coefficient k_a^{aer}. The extinction coefficient k_e, the scattering coefficient k_s, and the absorption coefficient k_a of the atmosphere are then given by [38]:

$$
\begin{aligned}
k_e &= k_e^{\ air} + k_e^{\ aer} \\
k_s &= k_s^{\ air} + k_s^{\ aer} \\
k_a &= k_a^{\ air} + k_a^{\ aer}
\end{aligned}
\tag{8.47}
$$

The state of the MRR is controlled by the data bits of "0" or "1" which for example are corresponding to the "off" and "on" states of the amplitude modulator, respectively. The receiver captures the retroreflected modulated beam and the data is decoded.

When the state of the MRR is "on", the retroreflective power at the receiver can be written as [38]:

$$
\begin{aligned}
P_r &= P_t \eta_t \exp\left(-k_e L\right) \frac{A_{retro} \cos\phi}{L^2 \Omega_t} \eta_{retro} \exp\left(-k_e L\right) \frac{A_r}{L^2 \Omega_{retro}} \eta_r \\
&= P_t\, \eta_t\, \eta_{retro} \eta_r \cos\phi \exp\left(-2k_e L\right) \frac{A_{retro} A_r}{L^4 \Omega_t \Omega_{retro}}
\end{aligned}
\tag{8.48}
$$

The parameters of the above equation are: interrogator laser power, P_t; wavelength, λ; transmitting beam divergence, θ_t; solid angle, $\Omega_t = 4\pi\, sin^2\left(\dfrac{\theta_t}{4}\right)$. For the receiver, the parameters are: detecting area, A_r; FOV, θ_t; solid angle, $\Omega_r = 4\pi\, sin^2\left(\dfrac{\theta_r}{4}\right)$; The range between the transmitter and the receiver is r. The parameters for the MRR: effective area, A_{retro}; incident angle on the MRR, ϕ; retroreflected beam divergence, θ_{retro}; solid angle of the MRR beam, $\Omega_{retro} = 4\pi\, sin^2\left(\dfrac{\theta_{retro}}{4}\right)$; the optical efficiencies of the laser interrogator, the receiver, and the on-state MRR are η_t, η_r, η_{retro}, respectively. The communication range is L. Air molecules suffer Rayleigh scattering and aerosol particles show Mie scattering effect. Figure 8.17 shows the results of the individual contributions of the retroreflective and scattering powers as a function of the communication range. The retroreflective power decreases sharply with

Fig. 8.17 Contributions of retroreflective and scattering signal powers as a function of the communication range (*Reprinted with permission from The Optical Society of America (OSA), 2012* [38])
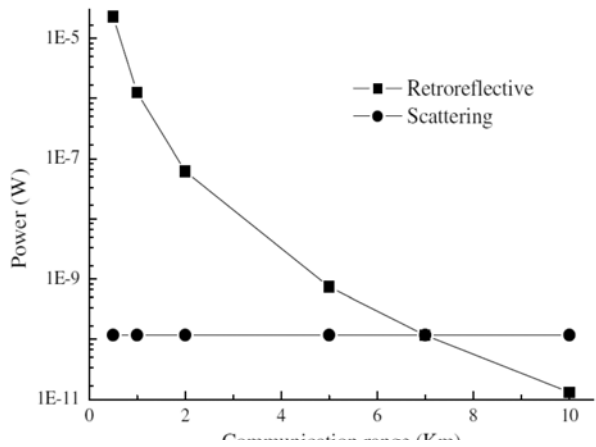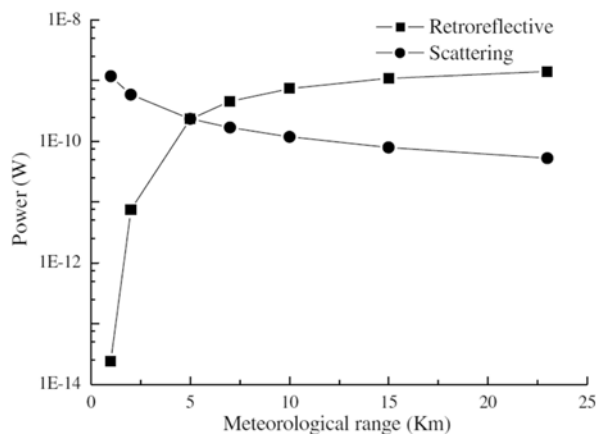
Fig. 8.18 Contributions of retroreflective and scattering signal powers as a function of the meteorological range (visibility) (*Reprinted with permission from The Optical Society of America (OSA), 2012* [38])

increased communication range, whereas the scattering power remains constant for this range.

Figure 8.18 shows the relationships between the retroreflective and scattering powers as a function of the meteorological range, sometime called "visibility." When the meteorological range decreases (i.e., visibility becomes poorer) the retroreflective power decreases correspondingly, while the scattering power increases instead, as expected for a poor visibility situation. Therefore, for a short meteorological range or poor visibility condition, the scattering power can overload a high-sensitive receiver. The MRR-based FSO communications system which has to operate under mostly scattering conditions need to be accordingly designed in terms of FOV of the receiver optics, interrogator laser power, range and other system parameters. In conclusion, in designing MRR-based FSO communications system, the scattering power, in addition to the retroreflective power, must be taken account

in the trade-off study, especially when the communication range is long or the meteorological range is short (low visibility).

8.6   Applications

MRR-based FSO communications is an exciting area with applications in many areas of commercial, biomedical, search and rescue, and industrial fields. The niche area of MRR-based free-space laser communications and data links is growing. We conclude this section by providing some examples of some recent experimental demonstrations performed by researchers and also some potential applications. Some of these applications are discussed below. The earlier sections provide the necessary backgrounds and analysis so that the readers can have full appreciations for the applications. Some of the MRR-based FSO communications applications include:

a. Ground-to-air and air-to-ground communications: real-time video transfer from UAV, Interspacecraft optical communication and navigation (guidance control for free-space platform, secure communication
b. Remote-telemetry applications: includes Mini-Rover (which was built for NASA's international space applications, it will move in the exact pattern display some data as sound and images, is an internet controlled robot
c. Locate objects of interest in a widely dispersed area, optical tagging (for tagging identification for remotely located consumables)
d. Autonomous mobile robot communication
e. Underwater optical communications
f. Car-to-infrastructure communication (telematics, car safety), communications for a vehicle, vehicle-to-vehicle optical two-way communication, FLC-based, MQW-based, fiber-retro-based
g. Optical tags (identification, sensors,)
h. High-speed wireless local area networks (WLAN)
i. Medical applications, human body transdermal optical wireless communications
j. Intra-office communications
k. Internal electronics bus interaction/communication

Retro-modulator laser communication from high altitude balloon platform The viability of retro-modulation communications was demonstrated for the first time by Swenson et al., [39] that performed the first passive retro-modulation experiment. Swenson et al. using FLC-based modulator and achieved a downlink at 12 Kbps data rate and used time division multiplexing to achieve bi-directional communications in a ground breaking experiment. A FLC-based retro-modulator is a low power 2 mW with accepted angles approaching 45° (half angle). For space applications this type of MRR satisfies the critical requirements such as large area, large acceptance angle, and low power, but speed and modulation depth at higher frequency are very low. The details of the FLC for retro-modulation were already

described in the text. The balloon reached a float altitude of 31 km and collected the modulated light reflected from the payload. A concept of a retro-modulator communications link where the remote site is a low-earth orbiting satellite was also illustrated by Swenson et al.

Data link between an UAV and ground station MQW modulating retroreflector (discussed earlier section of the text) was used by Gilbreath et al. [30] to demonstrate an IR data link between a small rotary-wing UAV and a ground based laser interrogator using the NRL's MQW retro-modulator. An Mbps optical link to a UAV in flight at a range of 100–200 ft was shown feasible, and near real-time compressed video transfer was demonstrated at the Mbps rate. Video or other forms of data can be obtained onboard the UAV and can be suitably modulated by the MRR using an appropriate format, and can retroreflect the video signal back when interrogated by a laser/receiver system. Instead of a single MQW MRR, if an array of MRR is used, the pointing requirements are considerably relaxed and the onboard FOV can be increased to accommodate the incoming beam with relaxed steering requirements. The communication package is thus very lightweight without heavy gimbaled mount and power supply and can be used for very small platforms. An InGaAs transmissive MQW modulating retro-modulator of 0.5 cm diameter was used for field tests by placing the MRR on the tail of the UAV pointing down. The six-element array of MRR was used. The UAV was flown at an altitude of 35 m. The NRL MWQ based MRR was demonstrated to support over 10 Mbps in a high signal level and captured data rates of 400 kbps and 910 kbps on a UAV in flight. Also near real-time color video using Joint Photographic Experts Group (JPEG) compression was demonstrated at a 1.2 Mbps. Results of an updated development of MQW retro-modulators for real-time video transfer using an array of devices was reported where color video using wavelet compression at 15 and 30 frames per second was achieved at 4 to 6 Mbps over 30 m in the laboratory [11]. Results at 1550 nm devices were also presented using "Cat's Eye Retromodulator." Real-time color video for a retro-modulator link of 2 m in the laboratory was also demonstrated at 3 Mbps and at 30 frames per second [40]. The device consumed about 75–100 mW and was 10 g.

Researchers have reported [41] the design of a free-space laser communication system from UAV to ground stations using MRR technology resulting in considerable reduction of power, size and weight onboard the UAV. The burden moves to the ground station but the acquisition, tracking and pointing subsystem requirements are also relaxed since the MRR acts as a pointing reference by reflecting the incoming laser beam back to the source. MEMS-based MRR was considered for achieving the data rate in the order of hundreds of Kbps and also high data rate communications with UAVs where the ground laser transmitter to be OOK-modulated at hundreds of Mbps. MEMS-based modulator is a reflective diffraction grating with controllable groove depth acting as one of the three mirrors of the retroreflector device. MEMS modulator is capable of modulating a CW laser beam by switching between an unpowered flat-mirror state to an energized-diffractive state.

The MRR technology allows transfer of information from UAVs permits communication to buoys on the water surface for information exchange and also to ve-

hicles on the ground. One single MRR can be interrogated simultaneously by many lasers. A peer-to-peer sensor network architecture using space-division multiple access (SDMA) and time division multiplexing (TDM) with optical retroreflectors is described in a report [42]. Retroreflector link in FDX mode operation is discussed.

MRR applications for Satellite Communications systems MRR devices are small and allow low powered, high data rate communications downlinks from small satellites. For space-to-space intersatellite links one satellite could be a microsatellite or smaller (Nanosat). For CubeSats, communications often dominate the power budget where MRR technology can be used. For small satellites, the ideal communication system is suggested [43] that would feature a space segment that allows high bi-directional data rates with low power consumption. A highly asymmetric system architecture using MRR devices as the transmitting element in the space segment was discussed.

Interspace laser interrogation, communication, and navigation between spacecraft platforms A novel concept utilizing MQW modulating retroreflectors to provide inter-spacecraft laser interrogation, communication, and navigation was described by Gilbreath et al. [44, 45]. An MRR enable compact, low power, and low mass optical data transfer on the order of Mbps, and relative navigation on the order of centimeters in three-axis position and arcminutes in two-axis tilt orientation was discussed. For docking missions where a close proximity operation of about 10 m are needed, the concept can work with a vision-based system.

Optical Tagging of a remotely located object An MQW retro-modulator array used as a low power, lightweight means to provide optical tagging of a remotely located object was reported by Gilbreath et al. [46]. Tagging identification was performed by demodulating the retroreflected signal using appropriate code. An array of 1/2 cm MQW devices was used at a range of about 40 m. MRR can have a potential solution for locating and identifying consumables such as food, and fuel in orbit which will be required for future long-range manned NASA missions. The MRR technology concept will also be useful as an aid for acquisition and tracking. The system can be very robust for space applications for supporting faster data rates, hence longer ranges, at lower powers than other existing devices. A MEMS-based optical tag was reported [47] in a laser communication experiment over 1 km optical range. The concept was based on employing interference to provide modulation to achieve modulation by tuning a large array of Fabry-Perot cavities via the application of an electrostatic force to adjust the gap between a movable mirror and the underlying silicon substrate. The MEMS based optical modulator was used to act as an interference switch in a modulated retroreflected tag with a bit rate of 200 Kbps.

Mobile Robot Communication MRR technology has applications for autonomous mobile robotic communication by establishing optical links to a small robot. Small robots can be used for operations in areas that may be hazardous and dangerous to humans and the robots can return video and other data from remotely located areas using high bandwidth optical communications. A single MRR will need about 1 degree pointing accuracy for operating at rates of Mbps at ranges of 1 km which

requires an active pointing and tracking. An array of 6 MRRs and photodetectors with FOV of 180° (azimuth)×30° (elevation) mounted on a small robot was described [48]. A 1.5 Mbps optical Ethernet link was established to a range of 1 km. The system worked at 1550 nm wavelength for maximum eye safety using transmits aperture of 2 in. and interrogator power of 350 mW. A transceiver board layout and its performance was described for autonomous mobile robotic application [49]. The robots were autonomous and needed to coordinate themselves without some sort of master. For robotic applications exchanging information such as position, speed, braking, turning, dimensions, and destination of the robot are essential. MRR technology can be used for this purpose. The maximum communication range achieved by the retroreflector robot was 60 ft. High data rate communication links in stationary or mobile mini-sensor suites using retro-modulator simulated on a mini-rover was demonstrated [50]. The host platform consumption of 50 mW and mass of 50 g were used for the communication subsystem. A typical example for use of this technology would be to establish communication link between a spacecraft, landed on a planet, with tens to hundreds of sensors or sensor carrying mini-rovers, distributed in the surrounding area.

FDX Communication on a Single Laser Beam The first experimental demonstration of FDX communications on a single laser beam was described by T. M. Shay et al. [51, 52]. The FDX optical communications means that a simultaneous bi-directional transmission is accomplished. The forward link beam (i.e., interrogating laser beam) simultaneously transmits the forward link data and serves as the carrier wave for the return link. MRR modulates the incident forward link beam according to the input data and is retroreflected back to the interrogator laser (receiver location). The photo-detector near the MRR serves as a receiver for the communication link from the transmitter (laser interrogator) to that receiver. The MRR is the transmitter for the receiver at the interrogator location. Thus a pair of Tx-Rx at both ends is possible which makes FDX operation. The forward data format must deliver a constant average power to the passive terminal and the return data format must be selected so that the forward data is invisible to the return link detection system. Shay et al. demonstrated with sub-carrier-FSK modulation for the forward data link, and a Circularly Polarized Keying [53] (CPK) for the return link. A diode laser interrogator transmits a linearly polarized beam which is then converted to a circularly polarized beam after passing through a quarter-wave plate, and the constant average power beam is sent to the MRR. The LC retro-modulator directs the incident beam back to the interrogator location and assigns left-handed and right-handed circular polarizations to the return beam according to binary data bit information. The LC will flip the right-handed polarized transmitter light into left-handed for a "1", while for a "0" the incident is unchanged. A second quarter-wave plate converts the returned left and right-handed circularly polarized beams into two orthogonally polarized beams respectively. A polarizing beam splitter separates the two orthogonal linear polarizations. The return signal photons, after passing through an optical filter are incident on the receiver located at the interrogator. The LC shutter was made from phase-separated composite films LC shutter with extinction ratio falling off rapidly

with frequencies beyond 20 kHz, consumed 1/2 W of electric power for unbiased data, and an extinction ratio of less than 3.5 % at 20-Kbps. A subcarrier-FSK modulation was selected for the forward data link and the return data format can be OOK modulation. This type of MRR- FSO communication concept has an application for earth-to-low-earth-orbit (LEO) optical system which can offer lightweight, low power consumption, low data rate communications from LEO satellites.

Fiber-based 2.5-Gbps ARM for FSO Communications   The concept of ARM using a high efficiency FSO-SMF coupler was described earlier in the text. The application includes the potential high data rate (~2.5 Gbps) FSO communications [51]. The optical amplifier increases the effective area of the retro-modulator by a factor of 318 and thus can provide the same return signal with a dramatic reduction in the system size and weight of the retro-modulator system.

Wide FOV Amplified Fiber-Retro for Secure High Data rate communications and Remote Data Transfer   The concept of this technology was described earlier in the text. The patent [54] describes the application of the concept to an optical system for remotely communications at a high data rate between a base station and a remote station under atmospheric conditions. The remote station includes retroreflectors consists of two sets of lenslets coupled with single-mode fiber array, called "fiber retro". Amplified retro modulation is achieved requiring only one single optical amplifier and one single modulator. A transmitter located at the base station sends an interrogating optical beam to the "fiber retro" which modulates the optical beam according to the input signal/data, and redirects the modulated optical beam to the base station for detection by a receiver. This technology includes the capabilities of providing Identification of Friend-or-Foe (IFF), secure communication, and a means of achieving a wide FOV with a fiber-coupled lenslet array. The simulation result shows the application of this technology for a satellite-based laser interrogator and ground-based amplified retro-modulator. The range of the satellite in the simulation was assumed to be 370 km the atmospheric transmission efficiency of 0.5, the BER $=10^{-9}$, SNR $=144$, and the gain of the retro-modulator system was taken to be 4×10^5. Results show that to achieve a data rate of 2.5 Gbps, for a transmitter divergent beam of 6.8 mrad, it requires only 160 mW of laser power, whereas for transmitter divergent beam of 27 mrad, it requires about 25 W of laser power. All these numbers are very practical and realistic and show the utility of ARM system concept.

Underwater Optical Communications using a MRR   Communicating with underwater sensors and vehicles is important in ocean exploration and observation. Underwater optical communication is possible at short ranges when application requires high data rates, low latency or covert operation. Optical scattering and absorption in the underwater environment limit the systems operation. Point-to-point optical links can have ranges approaching 200 m in clear water. A modulating retroreflector can be used with a laser on one interrogating platform (such as a submarine or unmanned underwater vehicle). The power-constrained platform (sensor node or small unmanned vehicle) acts as source to transmit the light beam towards a MRR.

The system can be designed to have duplex optical communication at low power. Researchers built an MRR that uses Fabry-Perot optical cavity for modulating light in the visible wavelengths for underwater communication where the intensity of the reflected or transmitted light can be modulated by electrically changing the cavity spacing [55]. Data transfer at rates of 250, 500 and 1 Mbps were demonstrated with a quadrature phase-shift keying (QPSK) modulation format. Another scenario for underwater modulating retroreflection communication link can be when one party (for example, a submarine) with more power consuming resource than another one (for example, a diver) [56]. Power requirements and the system complexity can then be put into the submarine and the diver can be equipped with a small modulating retroreflector and can collect information which can be obtained by the illuminating interrogator.

Remote Telemetry using MEMS Deformable Micromirror Array-based MRR MR concept can be used for remote telemetry application which includes remotely interrogated environmental sensors distributed over a large geographic area, and secure communications link. A laser interrogator can be mounted in an aircraft flying over the large area to interrogate the sensors remotely. The communication range for remote telemetry may extend from 0.1 to 10 km and must operate under varying environmental conditions. The system needs to operate over a wide range of incident angles, up to $\pm 30°$ which is possible with a hollow corner-cube retroreflector. An MRR was described [19] with one MEMS mirror that deforms from a flat into a hexagonal array of concave reflective microlenses to disperse the retroreflected wave front. A gold-coated silicon-nitride membrane suspended over 1-mm diameter circular cavities with a 79 V applied with a modulation contrast ratio of 7:1 and achieved 100-kHz modulation over a 35° range of incident angle.

Medical Application: Retroreflective Transdermal Optical Wireless Communication MRR link is an attractive communication solution in medical applications. Transdermal high data-rate communication for use in-body devices, such as pacemakers, smart prostheses, neural signals processors at the brain interface, and cameras acting as artificial eyes as well as for collecting signals generated within the human body are just some examples. Researchers have explored the potential of retroreflected optical link as a transdermal communication modality and have examined the channel characteristics [57]. MRR is attractive solution in medical applications because of its low power consumption in the order of μW. Another biomedical application involves especially implanted brain-computer interfaces which give rise to large data sets that needs to be transmitted transcutaneous. A link at near-IR (~854 nm) can be established using an MRR in the implant, but keeping the laser and the detector on the outside [58]. The modulator and drive electronics are the only part of this system that needs to be implanted.

Some applications using MRR technology were discussed. However there are more applications to explore. Some of them include: a communication link comprised of a Helmet-mounted and vehicle-based retro modulator, vehicle-to-vehicle optical two way communications, car-to-infrastructure communication (telematics,

traffic safety), internal electronics bus interaction/communication, intra-office communications and Industrial Manufacturing. The readers might find them interesting.

References

1. B.E.A. Saleh, M.C. Teich, *Fundamentals of Photonics*, Chap. 18, Electro-Optics (Wiley, Hoboken, NJ, 1991)
2. T.A. Maldonao, *Handbook of Optics*, Vol. II, Chap. 13 (McGraw-Hill, New York, NY, 1995)
3. G. Spirou, I. Yavin, M. Wheel, A. Vorozcovs, A. Kumarakrishnan, P.R. Battle, R.C. Swanson, A high-speed-modulated retro-reflector for laser using an acousto-optic modulator. Can. J. Phys. **81**, 625–638 (2003)
4. E. Hallstig, Nematic liquid crystal spatial light modulators for laser beam steering. Dissertation, Faculty of Science and Technology, ACTA Universitatis Upsaliensis, Uppsala, Sweden, 2004
5. G.C. Gilbreath, W.S. Rabinovich, T.J. Meehan, M.J. Vilcheck, R. Mahon, R. Barris, M. Ferraro, I. Sokolsky, J.A. Vasquez, C.S. Bovais, K. Cochrell, K.C. Goins, R. Barbehenn, D.S. Katzer, K. Ikossi-Anastasiou, M.J. Montes, Compact light weight payload for covert data link using a multiple quantum well modulations retro-reflector on a small rotary-wing unmanned airborne vehicle. Proc. SPIE **4127**, 57–67 (2000)
6. G. Charmaine Gilbreath, W.S. Rabinovich, T.J. Meehan, M.J. Velcheck, M. Stell, R. Mahon, P.G. Goetz, E. Oh, J.A. Vesquez, K. Cochrell, R.L. Lucke, S. Mozersky, Progress in development of multiple-quantum-well retro modulators for free-space data links. Opt. Eng. **42**(6), 1611–1617 (2003)
7. M.L. Bierman et al., Design and analysis of a diffraction limited Cat's eye retroreflector. Opt. Eng. **41**(7), 1665–1660 (2002)
8. G.C. Gilbreath et al., Large-aperture multiple quantum well modulating retroreflector for free-space optical data transfer on unmanned aerial vehicles. Opt. Eng. **40**(7), 1348–1356 (2001)
9. G.C. Gilbreath et al., Progress in development of multiple quantum well retro-modulators for free space data link. Opt. Eng. **42**, 1611–1617 (2003)
10. G. Charmaine Gilbreath, W.S. Rabinovich, T.J. Meehan, M.J. Vilcheck, M. Stell, R. Mahon, P.G. Goetz, E. Oh, J. Vasquez, K. Cochrell, R. Lucke, S. Mozersky, Real time video transfer using multiple quantum well retromodulators. SPIE Proc. **4821**(61), 155–162, (2002). (Gilbreath et al., Real-time 1550 nm retro-modulated video link. Proceedings of the 2003 IEEE Aerospace conference, paper No. 1560, March, 2003
11. W.S. Rabinovich, P.G. Goetz, R. Mahon, L. Swingen, J. Murphy, G.C. Gilbreath, S. Binari, E. Waluschka, Performance of Cat's eye modulating retro-reflectors for free-space optical communications. Proc. SPIE **5550**, 104–114 (2004)
12. P.G. Goetz, W.S. Rabinovich, R. Mahon, L. Swingen, G.C. Gilbreath, J.L. Murphy, H.R. Burris, M. Fa Stell, Practical considerations of retro-reflector choice in modulating retro-reflector systems. Digest of IEEE LEOS summer Topical Meetings, 2005
13. W.S. Rabinovich, P.G. Goetz, R. Mahon, L. Swingen, J. Murphy, M. Ferraro, H. Ray Burris Jr., C.I. Moore, M. Suite, G. Charmaine Gilbreath, S. Binari, D. Klotzkin, 45-Mbit/s Cat's eye modulating retro-reflectors. Opt. Eng. **46**(10), 104001 (2007)
14. W.S. Rabinovich, J.L. Murphy, M. Suite, M. Ferraro, R. Mahon, P. Goetz, K. Hacker, E. Saint Georges, S. Uecke, J. Sender, Free-space optical data link to a small robot using modulating retro-reflectors. Proc. SPIE **7464**, 746408-1 (2009)

15. P.G. Goetz et al., Modulating retro-reflector laser com systems at the Naval Research Laboratory. IEEE Military communications conference-Unclassified Program-systems Perspectives Track, 2010
16. A. Guillen Salas, J. Stupl, J. Mason, Modulating retro-reflectors: Technology, link budgets and applications. 63rd International Astro-nautical congress, Naples, Italy, IAC-12, B4, 6B, 11, 2012
17. L. Zip-Schatzberg, T. Bifano, S. Cornelissen, J. Stewart, Z. Bleir, Secure optical communication system utilizing deformable MEMS mirrors. Proc. SPIE **7209**, 72090C-1–72090C-15 (2009). (L. Zip-Schatzberg, T. Bifano, S. Cornelissen, J. Stewart, Z. Bleir, Secure optical communication system utilizing deformable MEMS mirrors. Proc. SPIE **7318**, 73180T-1–73180T-12 (2009))
18. T.K. Chan, J.E. Ford, Retroreflecting optical modulator using an MEMS deformable micro-mirror array. J. Lightwave Technol. **24**(1), 516–525 (2006)
19. C. Jenkins, W. Johnstone, D. Uttamchandani, V. Handerek, S. Radcriffe, MEMS actuated spherical retro reflector for free-space optical communications. Electron. Lett. **41**(23), 1278–1279 (2005)
20. D. Peterson, O. Solgaard, Free space communication link using a grating light modulator. Sensor. Actuator. **83**(1–3), 6–10 (2000)
21. C. Luo, K.W. Goossen, Optical micro electromechanical system array for free-space retro communication. IEEE Photonic. Technol. Lett. **16**(9), 2045–2047 (2004)
22. T.K. Chan, Retro-modulators and fast beam steering for free-space optical communications. Ph.D dissertation, University of California, San Diego, 2009
23. T.K. Chan, J.E. Ford, Retro-reflecting optical modulator using an MEMS deformable micro mirror array. J. Lightwave Technol. **24**(1), 516–525 (2006)
24. K.W. Goossen, Micro machined modulator and methods for fabricating the same, US Patent. 6519073, 2003
25. A.M. Scott, K.D. Ridley, D.C. Jones, M.E. MoN.e, G.W. Smith, K.M. Brunson, A. Lewin, K.L. Lewis, Retro reflectors Communications over a kilometer range using a MEMS-based optical tas. Proc. SPIE. **7480**, 74800 L-1–74800 L-10 (2009)
26. P. Schultz, B. Cumby, J. Heikenfeld, Investigation of five types of Switchable retro reflector films for enhanced visible and infrared conspicuity applications. Appl. Optics **51**(17), 3744–3754 (2012)
27. F. Mugele, J.C. Baret, Electro wetting: From basics to applications. J. Phys. Condens. Matter **17**, R705–R774 (2005)
28. T.M. Shay, R. Kumar, 2.5-Gbps amplified retro-modulator for free-space optical communications. Proc. SPIE **5550**, 122–129 (2004)
29. G. Keiser, *Optical Fiber Communications*, 2nd edn. (McGraw-Hill, New York, 1991)
30. G.C. Gilbreath, W.S. Rabinovich, T.J. Meehan, M.J. Vilcheck, R. Mahon, R. Burris, M. Ferraro, I. Sokolsky, J.A. Vasquez, C.S. Bovais, K. Cochrell, K.C. Goins, R. Barbehenn, D.S. Katzer, K. Ikossi-Anastasiou, M.J. Montes, Compact, lightweight payload for covert data link using a multiple quantum well modulating retro-reflector on a small rotary-wing unmanned airborne vehicle. Proc. SPIE **4127**, 57–67 (2000)
31. A.K. Majumdar, T.M. Shay, Wide field-of-view amplified fiber-retro for secure high data rate communications and remote data transfer, US Patent, No. US 8,301,032 B2, date of patent Oct. 30, 2012
32. A.M. Scott, K.D. Ridley, Calculations of bit error rates for retroreflective laser communications systems in the presence of atmospheric turbulence. Proc. SPIE **5614**, 31–42 (2004)
33. L.C. Andrews, R.L. Phillips, C.Y. Hopen, *Laser Beam Scintillation with applications* (SPIE, Bellingham, Washington, 2001)
34. A.K. Majumdar, Free-space laser communication performance in the atmospheric channel. J. Opt. Fiber. Commun. Rep. **2**, 345–396 (2005)
35. A.K. Majumdar, J.C. Ricklin, *Free-Space Laser Communications* (Springer, New York, 2008)
36. L.C. Andrews, R.L. Phillips, *Laser Beam Propagation through Random Media*, 2nd edn. (SPIE, Bellingham, Washington, 2005)

37. N. Avlonitis, P.B. Charlesworth, Performance of retro reflector-modulated links under weak turbulence. IET Optoelectron. **6**(6), 290–297 (2012)
38. H. Yin, T. Lan, H. Zhang, H. Jia, S. Chang, J. Yang, Theoretical evaluation of scattering effect on retroreflective free-space optical communication. J. Opt. Soc. Am. A Opt. Image Sci. Vis. **29**(12), 2608–2611 (2012)
39. C.M. Swenson, C.A. Steed, I.A. DeLaRue, R.Q. Fugate, Low power FLC-based retro modulator communications system. Proc. SPIE **2990**, 296–310
40. G. Charmaine Gilbreath, W.S. Rabinovich, R. Mahon, L. Swingen, E. Oh, T. Meehan, P.G. Goetz, Real-time 1550 nm retromodulated video link. Proceedings of the 2003 IEEE Aerospace Conference, Paper No. 1560, 2003
41. A. Carraso-Casado, R. Vergaz, J.M. Sanchez-Pena, Free-space laser communications with UAVs. Report of RT Organization, # RTO-MP-IST-099
42. J.L. Gao, Sensor network communications using space-division optical retro-reflectors for in-situ science applications. IEEE paper, 0-7803-7651-X/03, 2003
43. A.G. Salas, J. Stupl, J. Mason, Modulating retroreflectors: Technology, link budgets and applications. 63rd International Astronautical Congress, Naples, Italy, # IAC-12.B4, 6B,11, 2012
44. G. Charmaine Gilbreath, N. Glenn Creamer, W.S. Rabinovich, T.J. Meehan, M.J. Vilcheck, J.A. Vasquez, R. Mahon, E. Oh, P.G. Goetz, S. Mozersky, Modulating retroreflectors for space, tracking, acquisition and ranging using multiple quantum well technology, Proc. SPIE **4821**, 494–507 (2002)
45. N. Glenn Creamer, G. Charmaine Gilbreath, T.J. Meehan, M.J. Vilcheck, J.A. Vasquez, W.S. Rabinovich, P.G. Goetz, R. Mahon, Interspacecraft optical communication and navigation using modulating retroreflectors. J. Guid. Control Dyn. **27**(1), 100–106, (2004)
46. G.C. Gilbreath, T.J. Meehan, W.S. Rabinovich, M.J. Vilcheck, R. Mahon, M. Ferraro, J.A. Vasquez, I. Sokolsky, D. Scott Katzer, K. Ikossi-Anastasiou, P.G. Goetz, Retromodulator for optical tagging for LEO consumables. Technical Report, NRL, 2007
47. A.M. Scott, K.D. Riley, D.C.Jones, M.E. McNie, G.W. Smith, K.M. Brunson, A. Lewin, K.L. Lewis, Retroreflective communications over a kilometer range using a MEMS-based optical tag. Proc. SPIE **7480**, 2009
48. W.S. Rabinovich, J.L. Murphy, M. Suite, M. Ferraro, R. Mahon, P. Goetz, K. Hacker, W. Freeman, E. Saint Georges, S. Uecke, J. Sender, Free-space optical data link to a small robot using modulating retroreflectors. Proc. SPIE **7464**, 746408-1 - 746408-9, (2009)
49. K. Alhammadi, Applying wide field of view retroreflector technology to free space optical robotic communications. PhD dissertation in Electrical Engineering, North Carolina State University, Raleigh, North Carolina, September 2006
50. H. Hemmati, C. Esproles, W. Farr, W. Liu, P. Estabrook, Retro-modulator with a mini-rover. Proc. SPIE **5338**,50 -56, (2004)
51. T.M.Shay, J.A. MacCannell, C.D. Garrett, D.A. Hazzard, J.A. Payne, N. Dahlstrom, S. Horan, The first experimental demonstration of full-duplex communications on a single laser beam. Proc. SPIE **5160**, 265–271 (2004)
52. T.M. Shay, D. Hazzard, S. Horan, J.A. Payne, Full-duplex optical communication system, U.S. Patent. No. US 6,778,779 B1, Aug. 17, 2004
53. T.M. Shay, D.A. Hazzard, *Circular Polarization Keying*, patent pending, Serial No. 60/170,889
54. A.K. Majumdar, T.M. Shay, US Patent No. US 8,301,032 B2, Oct. 30, 2012
55. W. Cox, K. Gray, J. Muth, Underwater optical commun ication using a modulating retro-reflector. http://www.sea-technology.com/features/2011/0511/retroreflector.php, 2014 Compass Publications, Inc., published in Sea Technology, Vol.52, Issue 5, p.47, May 2011.
56. S. Arnon, Underwater optical wireless communication network. Opt. Eng. **49**(1), 015001 (2010)
57. Y. Gil, N. Rotter, S. Arnon, Feasibility of retroreflective transdermal optical wireless communication. Appl. Optics **51**(18), 4232 - 4239, (2012)
58. M.Y. Abualhoul, P. Svenmarker, Q. Wang, J.Y. Anderson, A.J. Johansson, Free-space optical link for biomedical applications, 34th Annual International Conference of the IEEE EMBS, San Diego, California USA, pp. 1667–1670, 28 August–1 September, 2012